# The effect of updating scavenging and conversion rates on cloud droplets and ice particles in the TM global chemistry transport model

*Jason E. Williams, Gerd-Jan van Zadelhoff and M.P. Scheele*

Authors:          Williams, J.E.
                  Zadelhoff, G.-J. van
                  Scheele, M.P.

● ● ● ●

# The Effect of Updating Scavenging and Conversion Rates on Cloud Droplets and Ice Particles in the TM global Chemistry Transport Model

*Jason E Williams, G-J van Zadelhoff and M P Scheele*

## Contents

## *Abstract*

In this technical report we document the updates which have been made to the heterogeneous reaction data used online in the TM model for the calculation of Henry's Law Co-efficients. The hydration step which needs to be included for the correct partitioning of aldehydes is now included explicitly which results in increases in the fraction transferred into the aqueous phase. In addition, wet deposition of all aldehydes is now included in the model. This update reduces the resident [HCHO] by between ~2-10% as a result of a ~65% increase in the amount lost through wet deposition, where the largest loss occurs in the tropics between 20°N-20°S. The subsequently reduction in [$HO_2$] results in less in-situ formation of the peroxy-species $H_2O_2$, $CH_3O_2H$ and ROOH, which contributes to the ~3-5% decrease in the tropospheric burdens for these species,. For methylglyoxal, the wet deposition term becomes the second most important sink process in the model once included.

A second update is associated with the introduction of parameterisations for a more accurate description of the size (effective radius)of ice particles and the corresponding reactive surface area in the model. Moreover, the reactive surface area from cloud droplets is also explicitly introduced into the calculation of the heterogeneous conversion of $N_2O_5$ into $HNO_3$ on the surface of such particles. For TM4, this significantly reduces the loss of $N_2O_5$ compared to the original formulation, which subsequently increases both [$O_3$] and [$NO_3$]. This is associated, in part, with an erroneous calculation of the Liquid Water Content in TM4. For TM5 the effects are more modest, where the heterogeneous conversion rate of $N_2O_5$ into $HNO_3$ decreases by ~50%.

Finally the gas phase conversion of $N_2O_5$ into $HNO_3$ involving water vapour is introduced into the modified CBM4 mechanism and tested online. This reaction has previously been identified as a large source of uncertainty between the different chemical mechanisms adopted in global CTM's. Analysis of the chemical budget shows that in the presence of heterogeneous conversion routes the influence of this additional conversion term is rather negligible.

Comparisons against a host of different in-situ measurements shows that adopting the updates does not degrade the performance of the model, where improvements are made to the mid-tropospheric ozone burdens and HCHO in the lower troposphere.

It is recommended that the new heterogeneous reaction data and the parameterisations for the calculation of the micro-physical properties of ice particles are adopted across all versions of the TM model.

# 1. Introduction

The atmospheric lifetime of soluble trace gases is influenced by the extent to which they partition themselves between both the gaseous and condensed/solid phases. Once incorporated into cloud droplets or aquated aerosol particles these trace species may then react with either free-radicals, which are formed *in-situ*, or other solutes (such as transition metal ions (e.g.) $Fe^{2+}$, $Mn^{3+}$). The rates of such reactions in solution are orders of magnitude larger than the corresponding reactions that occur in the gas phase (Warneck, 2000) enhancing their removal rates. Moreover, once in solution such species may then be removed from the atmosphere via wet deposition in rainfall, which acts as a significant global sink when integrated over a typical year. Many previous modelling studies have been performed in order to assess the effects of heterogeneous scavenging on the composition of the atmosphere, ranging from relatively simple 0-D box model studies (e.g. Lelieveld and Crutzen, 1990; Walcek et al, 1997; Ervens et al, 2003; Hermann et al, 2005) to 1-D column models with vertical exchange and development of the boundary layer (Williams et al, 2001) to 3D global Chemistry Transport Models (CTM's) (e.g. Liang and Jacob, 1997; Dentener et al, 2002). In general, these studies have found that both the $HO_x$ and $NO_x$ budgets are perturbed via the efficient partitioning of reservoir species such as HCHO, $H_2O_2$ and $HNO_3$ into the aqueous phase. This impacts the production of tropospheric ozone by perturbing the $HO_x$ and $NO_x$ budgets. Therefore any global CTM must include such scavenging processes in order to be able to account for this efficient global sink process.

The uptake of any species into a cloud droplet is determined by the rate of phase transfer. This uptake is a multi-step process governed by the physical properties of the gaseous molecule, the interface (droplet/particle surface) and the condensed phase. This process maybe summarised as the diffusion of the molecule in the gas phase to the liquid interface, followed by the transfer across the interface (otherwise known as accommodation). A quantity that represents the probability of successful scavenging into a droplet is the mass accommodation co-efficient, commonly known as $\alpha$ (which ranges between 0 and 1). For chemical species that react rapidly in solution, phase equilibrium between the gas and liquid phases is never fully established. Moreover, not all air masses are well mixed, which may introduce chemical gradients at the droplet surface. An effective parameterization for phase transfer has been developed by Schwartz (1986), which accounts for gas-phase diffusion and calculates an effective rate of transfer:

$$k_{trans} = \left( \frac{r^2}{3D_g} + \frac{4r}{3v\alpha} \right)^{-1}$$

(1)

Where r is the effective radius of the droplet (cm), $D_g$ is the gas phase diffusion co-efficient (cm² s⁻¹), and v is the mean velocity of the gas molecules (cm s⁻¹). The value of the mass accommodation co-efficient ($\alpha$) is specific to each particular species and surface, where values are available for a host of different gases in the recommendations (e.g. Sander et al, 2006). This $k_{trans}$ value should then multiplied by a dimensionless quantity L, which is expressed in cm³ $H_2O$ per cm³ air, which typically ranges between $10^{-8}$ to $10^{-6}$ cm³ cm⁻³ (Jacob, 2000).

For longer-lived species a common way of representing the solubility of a gas in water is by the Henrys law co-efficient (Sander, 1999), which maybe expressed as:

$$K_H = \frac{c_a}{P_g}$$

(2)

Where $c_a$ is the concentration of any species in the aqueous phase, $\rho_g$ is the partial pressure of the species in the gas phase and $k_H$ is in units of [M/atm]. It may also be represented as a dimensionless ratio between the concentration of the species in the aqueous phase and the concentration in the gas phase by multiplying $k_H$ by RT, where R is the universal gas constant and T is temperature (°K). The solubility of any gas typically has a temperature dependency, which maybe expressed as:

$$k_H = k_H^\theta \ \exp\left(\frac{-\Delta H_{so\ln}}{R}\left(\frac{1}{T} - \frac{1}{T^\theta}\right)\right)$$

(3)

Where $\Delta H_{soln}$ is the enthalpy of solution for a particular chemical species and $k_H^\theta$ the resulting Henry's co-efficient at 298.15°K. Moreover, some species either dissociate once in solution (e.g.) strong acids such as $H_2SO_4$, or form complexes with the solute (i.e.) HCHO in $H_2O$. This essentially increases the fraction that maybe incorporated into solution, where the new equilibrium state is determined by what is commonly known as the effective Henrys law co-efficient (hereafter referred to as $k_H$(eff)). This maybe represented in the following way:

$$K_H(eff) = K_H\left(1 + K_{hyd}\right)$$

(4)

Aldehydes readily form hydrates meaning that the uptake of species such as HCHO and methygloxal (hereafter denoted as $CH_3COCHO$) is enhanced due to Eqn (4). This can then be converted into a transfer rate by using Eqn (5):

$$k_{trans} = RT\frac{K_H}{(1.0 + K_H)}$$

(5)

Where the equilibrium fractionation of any species between the gaseous and aqueous phases can be represented by Eqn (6), where L is again the dimensionless entity representing the LWC:

$$f = K_H * LRT$$

(6)

For surface reactions, the rate at which the species interacts with any cloud particles is represented by Eqn (7). This implies there is no phase transfer thus allowing the instantaneous loss of the products back into the gas phase. In order to account for this properly the reactive surface area density (SAD in cm²/cm3) must be taken into account:

$$k_{surf} = \left(\frac{r}{D_g} + \frac{4}{v\alpha}\right)^{-1} A$$

(7)

In this technical report we evaluate the impact of updating the $k_H$ values for soluble trace species which are included in the modified CBM4 mechanism (Houweling et al, 1998) and used online in the TM global chemical transport model. Moreover, for ice clouds parameterizations are introduced which calculate both the effective radii and SAD using ECMWF meteorological input data. In Section 2, a description of the TM4 model used for this study is given along with the various sensitivity runs. In Section 3 we provide details of the reaction data chosen for the updates to $k_H$ and show the resulting differences between the new $k_H$ values and those which are currently implemented, as well as providing a description of the new cirrus parameterizations adopted. In Section 4 we show the effect of applying the updated $k_H$ values in TM4 on the global composition of the troposphere and perform an analysis of the chemical budget terms for such species to show that the enhanced scavenging of HCHO also has implications for other trace species via perturbations to the $HO_x$ budget. In Section 5 we provide examples of the global distribution of ice particles calculated as a result of using the new cirrus parameterization online. In Section 6 we discuss the effects of updating the $N_2O_5$ heterogeneous conversion rates on the composition of the troposphere and examine the importance of the gas phase conversion of $N_2O_5$ into $HNO_3$. Finally, we summarize the main conclusions in Section 7.

# 2. Description of the TM4 model

The version of the TM4 model used for this study is identical to that described in Williams and van Noije (2008) apart from the following details. The vertical resolution has been expanded to 34 vertical layers in order to increase the resolution in the upper troposphere and through the stratosphere, with the horizontal resolution being 3° longitude by 2° latitude. The chosen simulation year is 2006 meaning that the 91 layer ECMWF meteorological analysis is used to drive the model. The nudging of the overhead ozone column is done using monthly mean ozone fields derived from the Ozone Monitoring Instrument and imposed on the climatology of Fortuin and Kelder (1998). For the anthropogenic emissions we adopt the sector segregated estimates for the year 2000 made available through the RETRO website (http://retro.enes.org). These are based on the TNO Emission Assessment Model (TEAM) and are segregated with respect to the sector from which the emission originates. The emissions from all sectors except transport are introduced between 0-200m above the ground. These are supplemented with inventories for $NH_3$ and $SO_2$ taken from the EDGAR-HYDE version 1.3 (van Aardenne et al, 2001). For ship emissions we adopt the estimates from Endresen et al (2003) and for aircraft emissions those from the AEROCOM project (Lee et al, 2002; Grewe et al, 2002). We inject road transport emissions in the lowest model layer and ship emissions evenly between the lowest two layers, which corresponds to the first 100m above sea level. For biomass burning emissions we use the monthly aggregated estimates from the GFEDv2 database (van der Werf et al, 2006) and apply the injection heights given in Lavoue et al (2000), except for in the tropics where we increase the injection height to 2km considering the evidence from recent satellite measurements of biomass burning aerosol particles over southern Africa (Labonne et al, 2007). These biomass burning emissions are given a daily cycle to mimic the increased burning in the afternoon, which has been observed from both different satellite instruments which have staggered overpass times (Boersma et al, 2008) and geo-stationary platforms (Roberts et al, 2009). For lightning $NO_x$ we apply the parameterization of Meijer et al (2001) which gives ~5.9 TgN for 2006, which is slightly higher than the most likely range of ~ 5Tg, but well within the current uncertainty range (Schumann and Huntrieser, 2007). For all runs we do not include specific emissions for $CH_4$ but impose a latitudinal gradient at the surface. It should be noted that non-eruptive volcanic $SO_2$ emissions are taken from Andres and Kasgnoc (1998).

| Sensitivity test | Details of the sensitivity test | Other Comments |
|---|---|---|
| BASE | No updates to the heterogeneous data | No updates to any heterogenous scavenging rates |
| KHENRY | Updates to the $K_H$ values of chemical trace species | $K_H$ values of $H_2O_2$, $CH_3OOH$ and $ROOH$. $K_H$(eff) values updated for HCHO and values for $CH_3C(O)CHO$ and ALD2 added |
| KHET | As for KHENRY except updates made concerning the scavenging of $N_2O_5$ on cloud droplets and ice particles | The $r_{eff}$ of the Ice particles is calculated using Fu (1996) and the SAD using Heymsfeld and McFarquhar (1996). For cloud droplets a $r_{eff}$ of 8μM is used and the SAD calculated assuming a spherical droplet. |
| KNEW | As for KHET except the gas phase conversion of $N_2O_5$ to HNO3 is added to the CBM4 chemical mechanism | Temperature and pressure independent conversion rate taken from IUPAC |

Table 1: Definitions of the sensitivity tests used to determine the effects of updating the heterogeneous reaction data in the TM4 CTM model.

For the biogenic emissions we use the 12 year average of Lathiére et al (2006) supplemented with emissions of biogenic CO and alkanes from Müller (1992). In the tropics (20°N-20°S) we distribute the isoprene emissions equally between the lowest two model layers and impose a diurnal variation on the emission to account for the effects of sunlight and temperature. In the TM model the monoterpene emissions are currently included as additional isoprene due to the lack of an explicit terpene species in the modified CBM4 mechanism (Houweling et al, 1998).

For the purpose of investigating the chemical effects of updating the heterogeneous rate data we define a number of sensitivity studies, which are summarised in Table 1. The sensitivity tests focus on the two different heterogeneous processes which are currently included in the TM model, namely the incorporation of longer-lived trace species in cloud droplets and conversion of $N_2O_5$ into $HNO_3$ on the surface of droplets and ice particles. A further sensitivity test is included to assess the importance of the gas phase conversion of $N_2O_5$ into $HNO_3$ involving water vapour.

# 3. Details of the Updated Heterogeneous Reaction data

The reaction data selected for introducing updates for the calculation of $K_H$ principally come from the compilation made by Sander (1999), which provides values for a large number of chemical species gathered from the literature. The values which are selected are summarized below in Table 2, where values based on laboratory measurements are given precedence rather than those estimated in previous modeling studies. When applied in the TM model, the scavenging for each species is scaled to the ratio of the molecular weight of the trace species and $HNO_3$, using rainout rates from the parameterization of Roelefs and Lelieveld (1995). The uptake of both $CH_3C(O)CHO$ and ALD2 have also been included for the first time.

| Chemical Species | $k_H^\theta$ [M/atm] | $\dfrac{\Delta_{so\,\ln} H}{R}$ | Reference |
|---|---|---|---|
| $H_2O_2$ | $1 \times 10^5$ | 6300 | Lind and Kok [1994] |
| $CH_3OOH$ | 310 | 5300 | O'Sullivan et al [1996] |
| ROOH | 340 | 6000 | O'Sullivan et al [1996] |
| $HCHO^*$ | 3000 | 7200 | Betterton and Hoffmann [1988] |
| $CH_3C(O)CHO^*$ | $3.2 \times 10^4$ | - | Zhou and Mopper [1990] |
| $ALD2^*$ | 17 | 5000 | Zhou and Mopper [1990] |
| | 13 | 5700 | Zhou and Mopper [1990] |

Table 2: Details concerning the heterogeneous reaction data introduced into the TM4 model in order to update heterogeneous scavenging rates. For the species containing a –CHO functional group (denoted by *) a hydration rate is also applied which further enhances the solubility in aqueous solution. For ALD2 an average is calculated from the uptake values for $CH_3CHO$ and $C_2H_5CHO$, whereas for ROOH the uptake value for $C_2H_5OOH$ is adopted.

In Figure 1 we compare the resulting change in $K_H$ values when applying the new reaction data with respect to temperature for the peroxy species that are listed in Table 2. For the temperature range that is relevant to the troposphere (280-310°K) it can be seen that all three $K_H$ values increase, with the largest increase being associated with $H_2O_2$. This translates into increases in $K_{trans}$ of between 5-60%. When applied online in a global CTM this has the potential to increase the fraction of each species that is scavenged into solution and, thus, the total loss by wet deposition. Moreover, the oxidation of $SO_2$ in cloud droplets is also likely to increase as a result of the enhanced phase transfer of $H_2O_2$. The most dramatic increase of all species is for HCHO where increases of between 200-300% occur (not shown). This is a result of the explicit introduction of the hydration step (i.e.) the introduction of $K_H(eff)$. For the remaining species no wet scavenging was included in the TM model before performing this update.
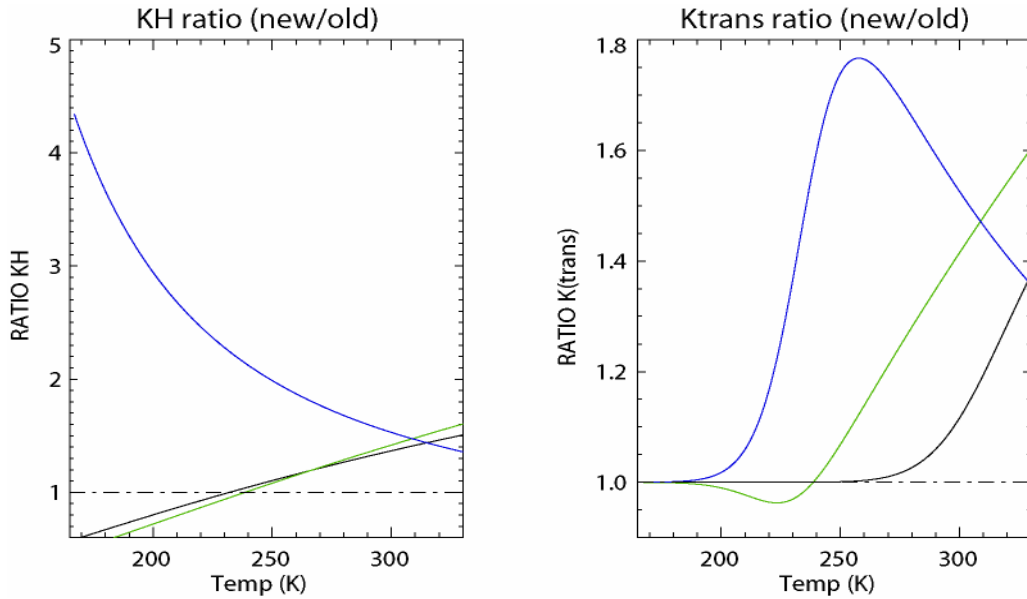
Figure 1: Ratios between the values of $K_H$ and $K_{trans}$ for $H_2O_2$ (–), $CH_3OOH$ (–) and ROOH (–) in the original TM code versus the updated values.

The uptake of $N_2O_5$ is treated differently from the other chemical species as it is considered to have a much shorter lifetime and therefore assumed not to undergo phase transfer but rather conversion on the reactive surface. Therefore Eqn (7) should be used to describe the conversion of $N_2O_5$ into $HNO_3$ (denoted as KN2O5L) rather than Eqn (5). The assumption that no uptake occurs has recently been brought into question as a result of observations in the laboratory related to the uptake of $N_2O_5$ into a variety of different tropospheric aquated aerosols (Bertram and Thornton, 2009). However, without adapting this new parameterisation for sulphate aerosols this cannot currently be included into the current default version of TM, which is beyond the scope of this study. For the input parameters for calculating $N_2O_5$ conversion the mean molecular velocity has been changed from the original value of 4.0 x 10$^5$ cm s$^{-1}$ to 2.4 x 10$^4$ cm s$^{-1}$ (J. Crowley, Personal communication, 2009), the uptake co-efficient on ice particles and cloud droplets is increased from 0.01 to 0.02 as recommended in the latest recommendations (Sander et al, 2006) and the $r_{eff}$ for cloud droplets reduced to 8μM throughout the troposphere, in line with the value used for accounting for the attenuation of light by cloud droplets in the photolysis routine of the TM model. For the SAD of each phase we replace the current formulation with the following: (i) For liquid droplets we calculate the SAD from the number of cloud droplets per cm³ air, multiplied by the surface area of each droplet assuming spherical geometry using a fixed effective radius of 8μM. (ii) For the ice particles the SAD is calculated by introducing the parameterization of Heymsfield and McFarquhar (1996), where the cross-sectional area is related to the Ice Water Content (g/m³) according to:

$$A_c = 10^{-4} IWC^{0.9} \tag{8}$$

The SAD is subsequently calculated assuming a scaling ratio which is applied to the cross-sectional area. The value of the scaling ratio using in previous CTM studies ranges between 2-4 (e.g Lawrence and Crutzen (1998), von Kuhlmann and Lawrence (2006)), as provided in Heymsfield and McFarquhar (1996). However, recent *in-situ* measurements by Popp et al (2004) suggest that the SAD can be significantly higher than this range of values. Recently, Schmitt and Heymsfield (2005) have suggested that the value should be ~10, which is representative of irregularly shaped particles and has been derived using measurements taken during the CRYSTAL-FACE and FIRE-II campaigns. Therefore, this more recent recommendation for the scaling ratio is adopted in this study. The fixed $r_{eff}$ value of 50μm which was previously adopted for ice particles is replaced using the parameterization of Fu (1996):

●  ●  ●  ●     6

$$r_{eff} = \frac{\sqrt{3}}{3\rho_i}\frac{IWC}{A_c} \qquad (9)$$

Here the $r_{eff}$ is given in cm$^{-1}$ and calculated using an IWC in g/cm$^3$. This parameterization for determining $r_{eff}$ has been shown to perform well versus measurements of cloud properties made both at the mid-latitudes and the tropics (Heymsfield, 2003). These values are subsequently used in Eqn. 7 for the calculation of the heterogeneous conversion rate of $N_2O_5$. To help the reader visualize the range in values for both $r_{eff}$ and SAD that are calculated by Eqns (8) and (9), Figure 2 shows how both quantities vary with the IWC product as provided by ECMWF, which is given in Kg H$_2$O/Kg air. It can be seen that the size of the ice particles is smaller than fixed value of 50μm used before across the entire range of IWC that typically occurs in the meteorological input data from ECMWF.



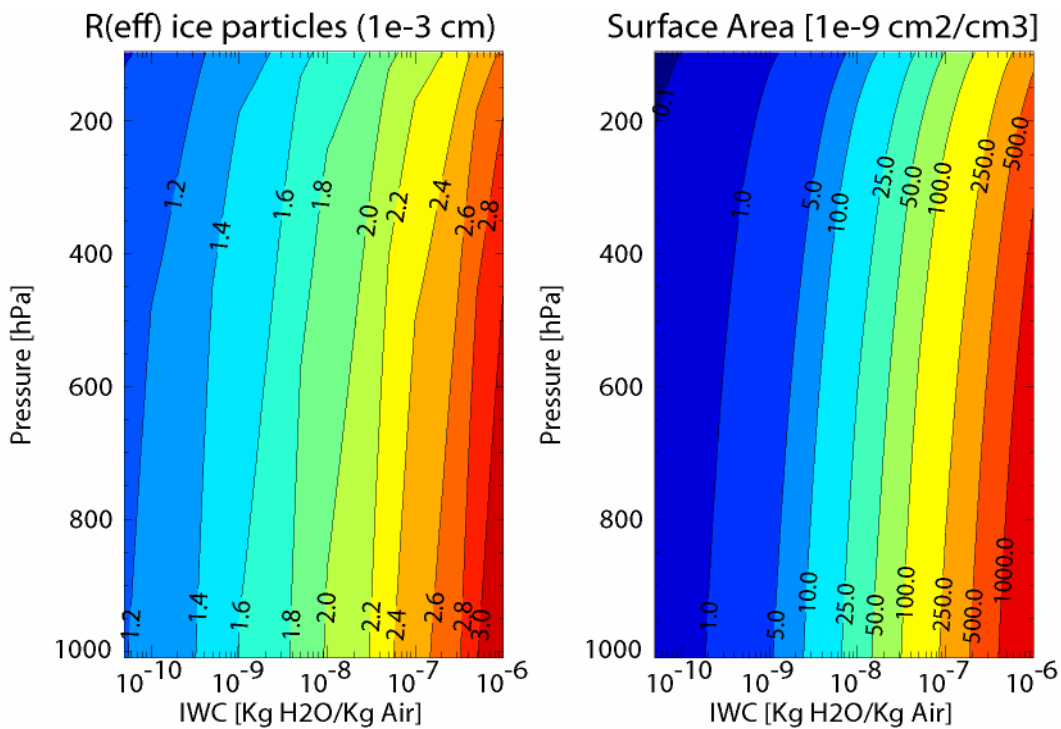Figure 2: The variation of the effective radii (10$^{-3}$ cm$^{-1}$) and surface area density (10$^{-9}$ cm$^2$/cm$^3$) for ice particles with respect to IWC as calculated using the parameterizations of Fu (1996) and Heymsfeld and McFarquhar (1996), respectively. The effective radius of ice particles was fixed at 5 x 10$^{-3}$ cm$^{-1}$ in the previous version of the TM code.

Figure 3 shows the variability in the magnitude of $KN_2O_5L$ as calculated using both the old and new methods. Here a fixed liquid water content (LWC) profile was used as calculated using ECMWF values for the tropics averaged between 20°S-20°N for all longitudes. By adopting this profile we introduce some variability in the SAD of the clouds throughout the column. As $KN_2O_5L$ has a contribution from both the conversion of $N_2O_5$ on ice and cloud surfaces, the dominant term changes with respect to height. For the lower to mid troposphere $KN_2O_5L$ is dominated by the cloud term, as shown by the lack variation in $KN_2O_5L$ with respect to IWC. For the upper troposphere, where the LWC is low, the SAD from the ice particles becomes the dominant term. Comparing the differences shows that, in general, the rate of $KN_2O_5L$ decreases by several orders of magnitude. This is principally due to a conversion error which was present in TM4 which produced LWC values three orders of magnitude too large. Considering that a pseudo first-order conversion rate rarely has values higher than 0.01 s$^{-1}$, the range of values calculated using the new parameterizations seem to be much more plausible. A further modification to the calculation of $KN_2O_5L$ is that the available SAD is now used explicitly, whereas before the dimensionless scaling quantity (L) was used to scale the product of Eqn (1). In

principle the use of this dimensionless quantity is only valid if phase transfer of the trace species is assumed to occur (c.f. Eqn (6)), where the kinetics in TM describes a surface conversion (i.e.) $HNO_3$ is released directly back into the gas-phase and does not remain in solution, which would constitute irreversible loss of nitrogen. Phase transfer of $HNO_3$ from the gas phase into droplets is described explicitly using the respective $K_H$ value. The method using the available surface area is given in Dentener and Crutzen (1993) for aquated aerosols, and also outlined in Jacob (2000) for application to cloud droplets. The application of the correct method has consequences for both the nitrogen oxide radical budget and the tropospheric ozone burden as discussed in Section 6. For TM5 the calculation of the LWC is performed correctly meaning that the differences in $KN_2O_5L$ are much smaller between the old and new approach, where reductions of ~50% occur.
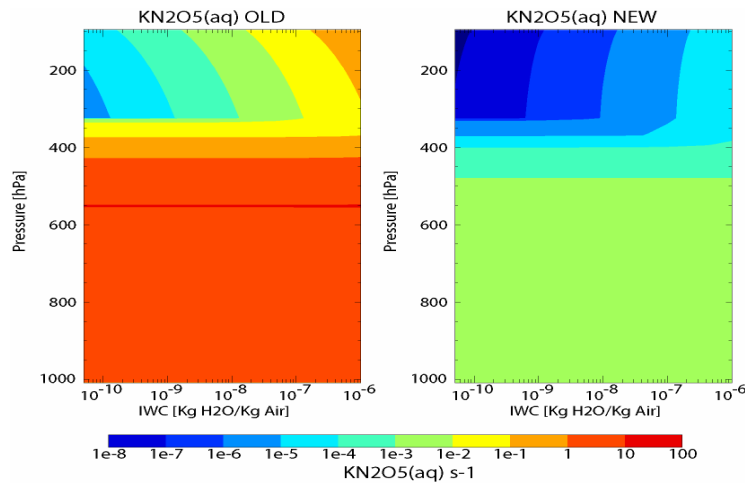


Figure 3: The variation of $KN_2O_5L$ throughout the troposphere calculated in TM4 with respect to IWC using both the old and new approaches for the calculation of reactive surface area of ice particles and cloud droplets. The LWC, pressure and temperature profiles are taken from monthly mean values for June 2006 near the Equator.

Figure 4 shows the corresponding variability in $KN_2O_5L$ with respect to LWC when using a fixed ice water content (IWC) profile for the tropics. Comparing the resulting $KN_2O_5L$ values shows that for TM4 there are again decreases of a few orders of magnitude in $KN_2O_5L$ in the lower troposphere. The most relevant values of $KN_2O_5L$ shown are associated with values for LWC in the range of $10^{-6}–10^{-4}$ below 700hPa. For TM5 the differences are again much smaller between the two approaches
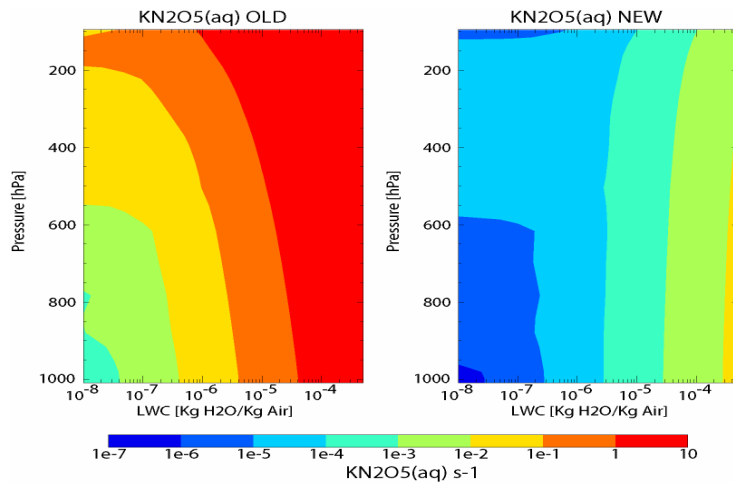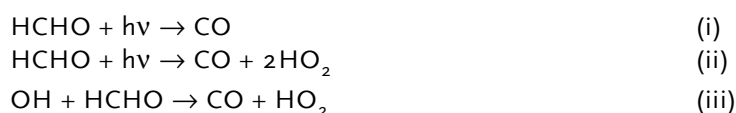


Figure 4: As for Figure 3 except differences are shown with respect to LWC.

# 4. The Effects on Enhanced Wet Deposition on Tropospheric Chemistry

In this section we examine the effect of updating the reaction data for the calculation of $K_H$ on the global distribution of $HO_x$ reservoirs in TM4 for the year 2006. For this purpose we make comparisons between seasonal means calculated using the monthly mean mixing ratios obtained during the BASE and KHENRY simulations for the tropical zones (20°N-20°S) in order to highlight which of the updates introduce the most significant effects. The tropics is chosen as ~70% of the total loss by wet deposition occurs in this latitudinal zone. Moreover, we also discuss the changes introduced into the global budget terms for the main $HO_x$ reservoirs and show how the updates influence the oxidising potential of the atmosphere by changing the $OH/HO_2$ ratio. The percentage differences discussed in the text below relate to those obtained by integrating globally throughout 2006.

## 4.1 Formaldehyde

Considering that the most dramatic increase in $K_H$ occurs for HCHO we discuss the effects on this species separately. The predominant chemical loss route for HCHO in the modified CBM4 mechanism is photo-oxidation, which accounts for ~67% of the total loss, where a further ~20% is oxidized by OH. These processes are described in equations (i) through to (iii) below:

$$HCHO + h\nu \rightarrow CO \qquad \qquad \text{(i)}$$
$$HCHO + h\nu \rightarrow CO + 2HO_2 \qquad \qquad \text{(ii)}$$
$$OH + HCHO \rightarrow CO + HO_2 \qquad \qquad \text{(iii)}$$

An analysis of the chemical budget shows that the loss of HCHO by wet deposition increases by ~65% from 115Tg HCHO yr$^{-1}$ to 190Tg HCHO yr$^{-1}$ when adopting the new uptake data. This large increase is due, in part, to the explicit introduction of the hydration rate into the rate parameters (i.e) the introduction of $K_H$(eff). There is an associated decrease in the global tropospheric burden of HCHO by ~10% when integrating through an entire year, which subsequently perturbs the global $HO_x$ budget by reducing the conversion of OH to $HO_2$ by ~4% due to Eqn (iii). The reduced burden also results in a corresponding decrease in the photo-oxidation of HCHO and oxidation by OH by ~6% and ~4%, respectively. Moreover, once oxidized HCHO produces additional CO which also contributes to the conversion of OH into $HO_2$, as described in equation (iv):

$$OH + CO \rightarrow HO_2 \qquad \qquad \text{(iv)}$$

Here the oxidation of CO acts as the most important chemical sink for OH in the troposphere. Thus, the net result is that every HCHO molecule which is oxidized by OH ultimately forms at least two $HO_2$ radicals making an appreciable contribution to the cycling of OH into $HO_2$. Comparing the global burdens for CO between the BASE and KHENRY runs reveals that there is a decrease of ~3.5% as a result of the enhanced loss of HCHO, which results in ~2.4% decrease in the conversion of OH into $HO_2$ by Eqn (iv).

Figures 5a and b show the seasonal differences in [HCHO] for June-July-August (JJA) for the tropics as averaged between 0-20°N and 0-20°S, respectively. For [HCHO] there are generally reductions of between ~5-10% throughout the entire troposphere, which essentially reduces the seasonal mean for [HCHO] by between ~100-200 pptv in the free troposphere. The highest losses occur above the strong source regions of South America, Africa and India, where the intensity and frequency of rainfall can be relatively high.
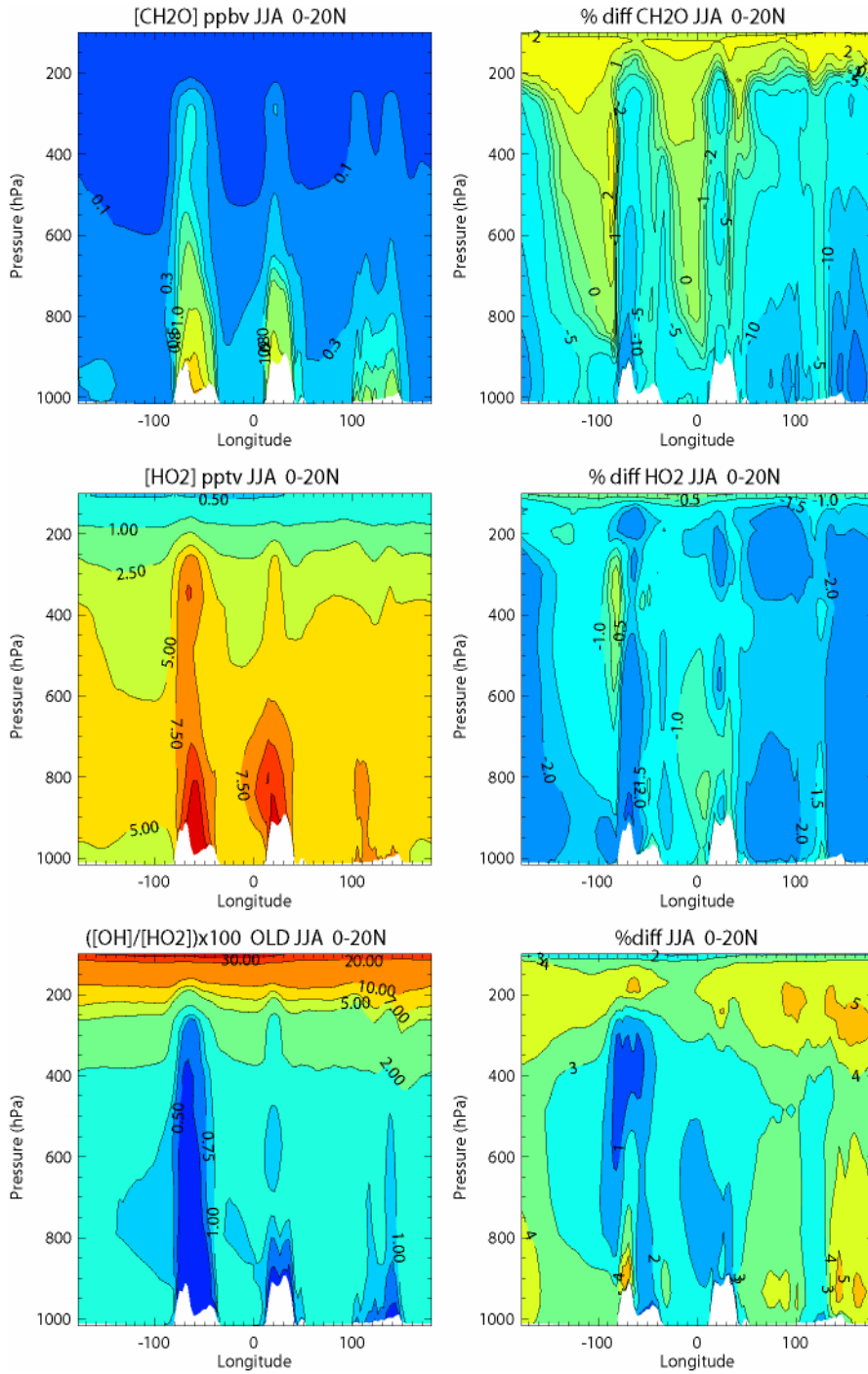
● ● ● ●　　9

Figure 5a: The tropospheric distribution and percentage differences in [HCHO], [HO$_2$] and the resulting ratio of [OH]/[HO$_2$] for season JJA during 2006 averaged between 0-20°N for all longitudes. The percentages are calculated for (KHENRY-BASE)/BASE. For the [OH]/[HO$_2$] ratio it is the difference between (RATIO$_{KHENRY}$–RATIO$_{BASE}$)/RATIO$_{BASE}$.
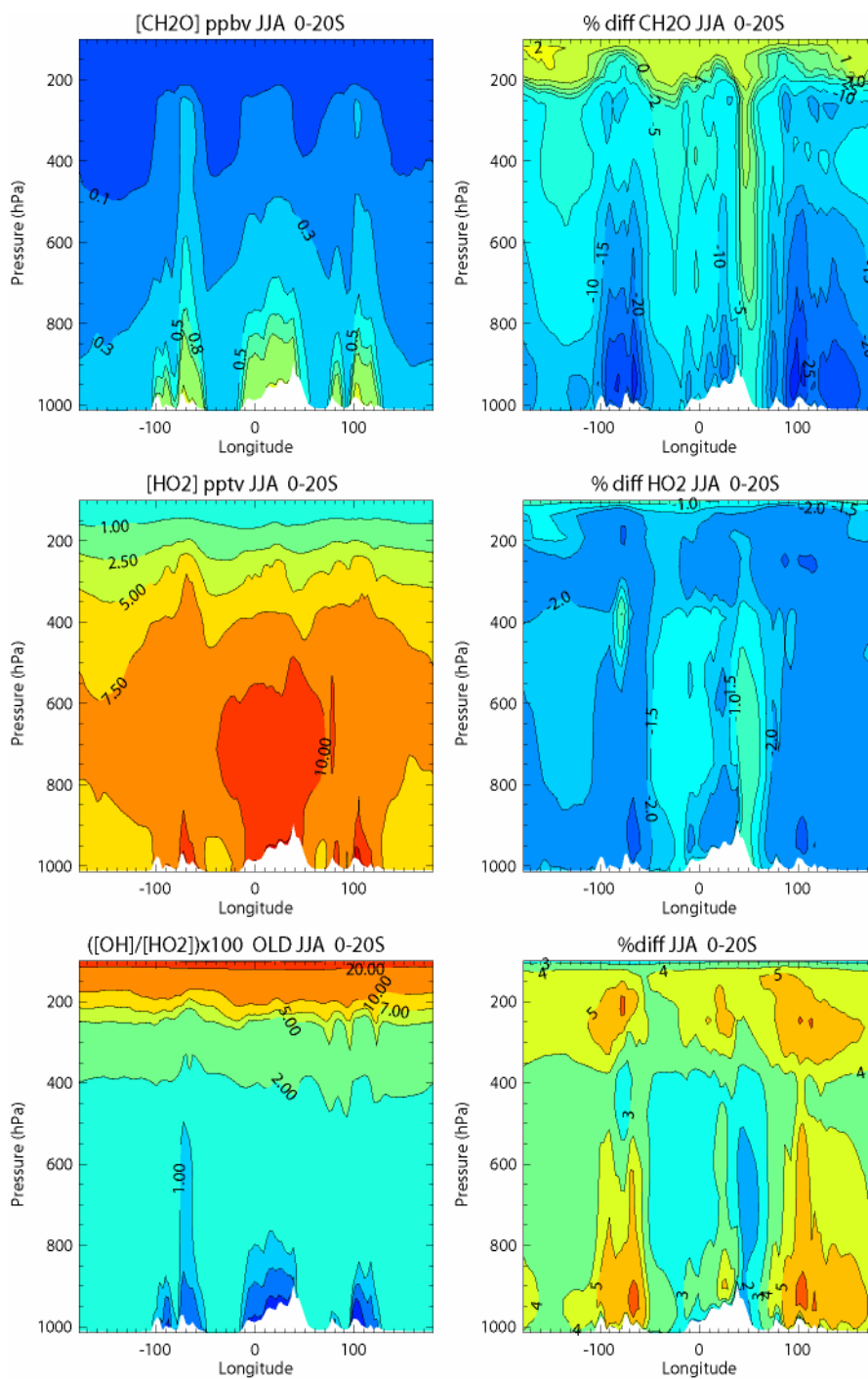
Figure 5b: As for Figure 5a except for the latitudinal region of 0-20°S.
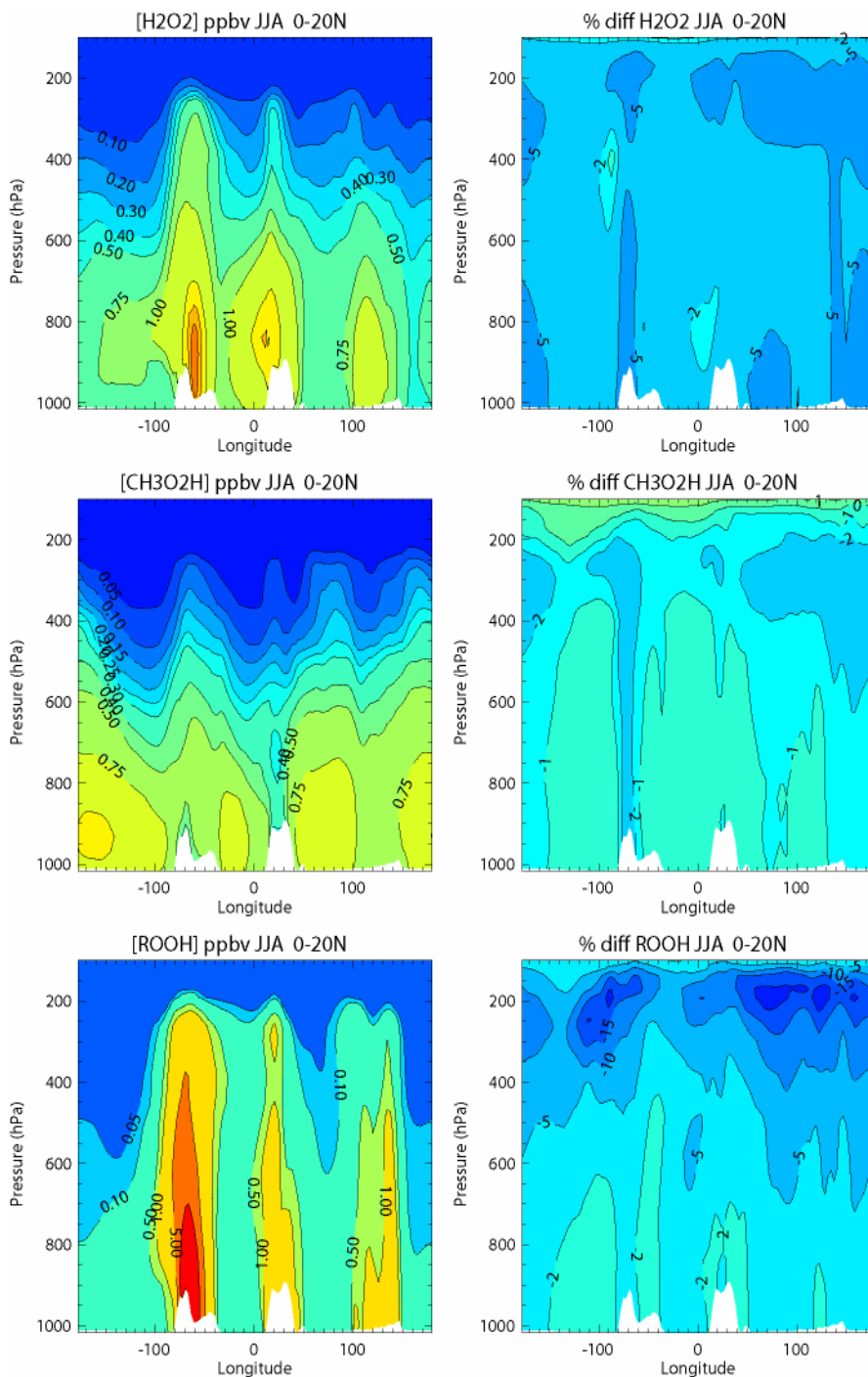
Figure 6a: The tropospheric distribution and percentage differences in [$H_2O_2$], [$CH_3O_2H$] and [ROOH] for season JJA during 2006 averaged between 0-20°N for all longitudes. The percentages are calculated for (KHENRY-BASE)/BASE.

Figure 6b: As for Figure 6a except for the latitudinal region of 0-20°S.

For [$HO_2$] there is an associated decrease of a few percent as shown in the middle panels. Finally, the lower panels show the resulting increase in the [OH]/[$HO_2$] ratio of between 1-5% due to the loss of $HO_x$ precursors, where the consequences for the oxidizing capacity of the troposphere are dealt with later in Section 4.4. For other latitudinal zones (e.g. 40-60°N) the results are rather similar except the concentrations of [HCHO] are generally lower.

## 4.2 Peroxides

Figures 6a and b show the corresponding seasonal differences for all three peroxy species during season JJA for the tropics as averaged between 0-20°N and 0-20°S, respectively. In general there are decreases in the tropics of between ~2-10% for all of the peroxide species that are included in the CBM4 mechanism. This is related to the cumulative effect of both a reduction in the *in-situ* chemical production terms and an increase in the loss by wet deposition. In order to differentiate the contributions of both terms we decompose the chemical budget terms for each of the three peroxide species in Appendix A, which reveals that there is a reduction in the *in-situ* chemical production of $H_2O_2$ and ROOH by between ~2-4% due to lower $[HO_2]$. For $CH_3O_2H$ there is a compensating effect in that the enhanced oxidation of $CH_4$ (due to less global [CO]) results in higher $[CH_3O_2]$ and the net production rate of $CH_3O_2H$ does not change to any significant extent. Therefore, the reduction in [HCHO] imposes a significant indirect effect on the resident concentrations of all peroxy species by reducing $[HO_2]$. The resulting global burdens for the peroxy species decrease by between ~3-5%.

For the loss by wet deposition, the largest increase occurs for $CH_3O_2H$ (~32%) reaching 62.2Tg $CH_3O_2H$ yr$^{-1}$. Again, this has a feedback on the formation of the other peroxides in that a major product from $CH_3O_2H$ oxidation is HCHO (see Appendix A). For $H_2O_2$ the reduction in the tropospheric burden results in a slight decrease of ~3% in the total mass lost by wet deposition, in spite of the increase in $K_H(H_2O_2)$. There is also a moderation in the increase in the loss via wet deposition for ROOH for the same reason.

## 4.3 Aldehydes

For $CH_3C(O)CHO$ and ALD2 the introduction of wet scavenging has markedly different effects as a result of the degree to which each species becomes hydrated in solution and their respective $K_H$ values. Performing similar comparisons to those shown in the figures above reveals that differences of between ~50-100% occur for $CH_3C(O)CHO$ and ~5-10% occur for ALD2 (not shown), although the resident $[CH_3C(O)CHO]$ is substantially lower than [ALD2]. This results in the loss of $CH_3C(O)CHO$ by wet deposition becoming the second most important term in the chemical budget (accounting for ~2.15Tg $CH_3C(O)CHO$ yr$^{-1}$). This results in an associated decrease in the oxidation by OH by ~16% and by photolysis of ~19%. For ALD2 the effect is more limited, where the loss by wet deposition is the least important sink only accounting for ~0.85Tg ALD2 yr$^{-1}$. There is also an associated reduction in the photolysis of ALD2 by ~18%. The reduction in the photo-dissociation of both these trace species also contributes to the global reduction in both CO and $HO_2$, which are directly formed (Houweling et al, 1998).

## 4.4 Long lived trace species

Here we focus on tropospheric $O_3$, CO and $CH_4$ which are the most long-lived and abundant trace gas species included in the TM model and whose chemical production/destruction is accounted for in the modified CBM4 mechanism. In order to diagnose the main changes to these key species we adopt an identical approach to that described in Williams and van Noije (2008) as taken from the ACCENT intercomparison exercises (e.g. Stevenson et al, 2006). The findings are presented in Appendix B and are a way of defining the changes to the chemical reactivity of the model and the reader is referred to these tables to support the following discussion. In general the model becomes less chemically active when applying the new rate data, where there is a reduction in the tropospheric ozone burden of ~0.5% due to there being a lower conversion rate of NO to $NO_2$ via the reaction with $HO_2$. For CO there is a reduction in the tropospheric burden of ~3.5% as a result of the enhanced wet deposition of HCHO (see discussion above). Analysis of seasonal means for various latitude bands shows that regionally this change in [CO] increases to ~5% in the tropics, whilst in the NH the difference is lower being between ~1-2% (not shown). Considering the importance of CO on the global OH budget any decrease in the total tropospheric burden of CO results in a different partitioning in the main chemical sink terms, which subsequently decreases the chemical lifetime of $CH_4$ by ~1%.

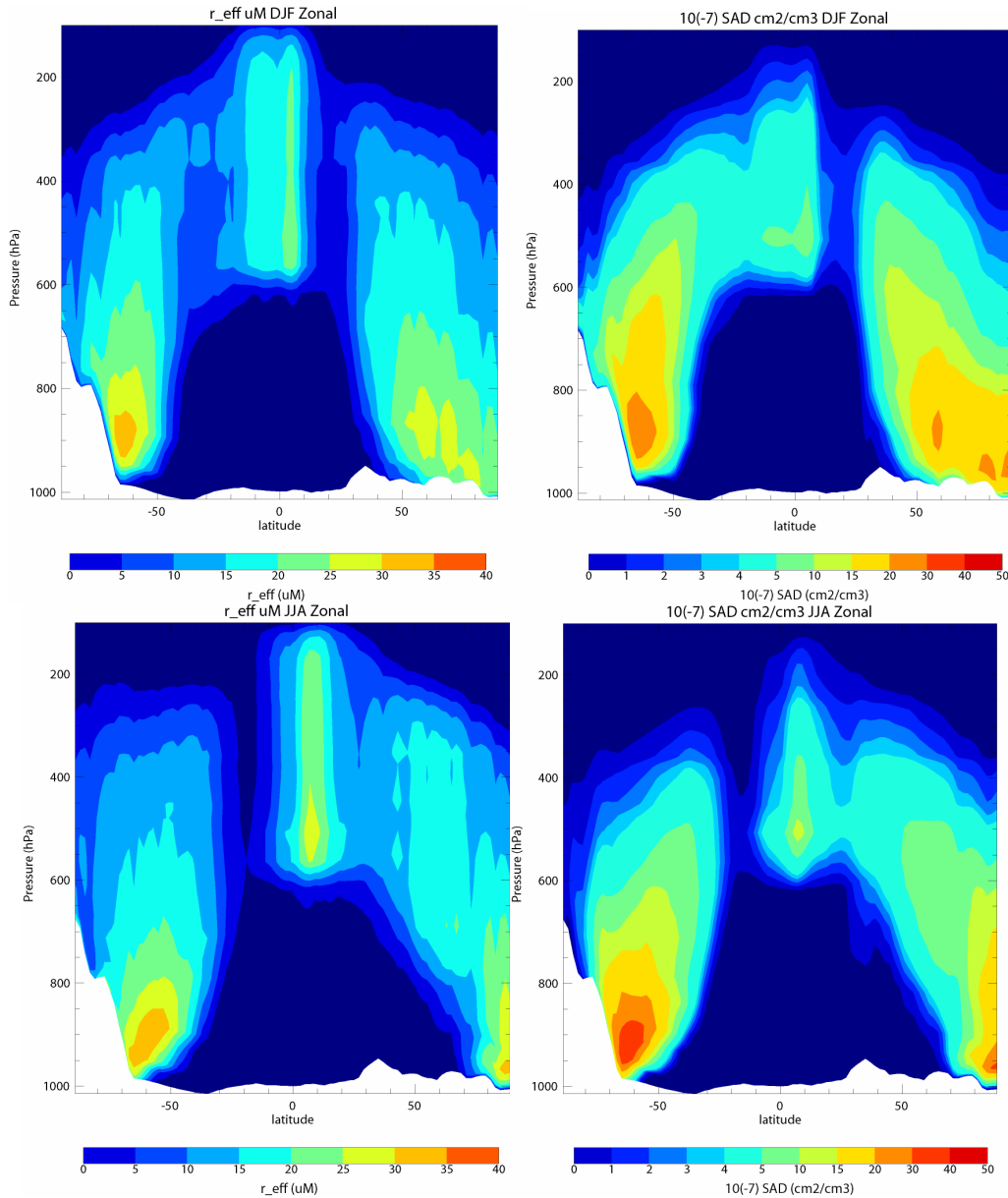# 5. The Global Distribution of Ice Particles and Clouds using ECMWF Meteorological Data



Figure 7: The zonal means of the effective radius and SAD of ice particles for seasons DJF (top) and JJA (bottom) during 2006. The occurrence of ice particles shifts towards the SH during DJF and the NH during JJA.

In this section we present some examples of the global distribution of ice particle sizes and the associated SAD values when Eqns (8) and (9) are applied online in the global CTM TM4, where the meteorological input variables are taken from the ECMWF operational dataset. Moreover, in Appendix C we present the seasonal variations of the main physical parameters used for calculating the heterogeneous conversion of $N_2O_5$ for a

number of different latitudinal zones. A threshold is applied during the calculation of ice particle coverage to instances where the cloud cover is <1% and the IWC < 10$^{-10}$ kg H$_2$O/kg Air.

Figure 7 shows the zonal seasonal mean values for both r$_{eff}$ and the SAD of the resulting ice particle fields for both December-January-February (DJF) and June-July-August (JJA). The largest particle sizes occur either in the tropical upper troposphere or in the lower troposphere at the poles, as dictated by the distribution in the IWC (not shown). Moreover, the maximum monthly mean radius that occurs is lower than the 50μM fixed radius adopted in previous versions of the TM model, which agrees with the changes in r$_{eff}$ shown in Fig. 2. It should be noted that by presenting a seasonal mean, it appears that particle sizes of < 10μM can occur whereas in fact there are instances during the averaging period where particles do not exist.
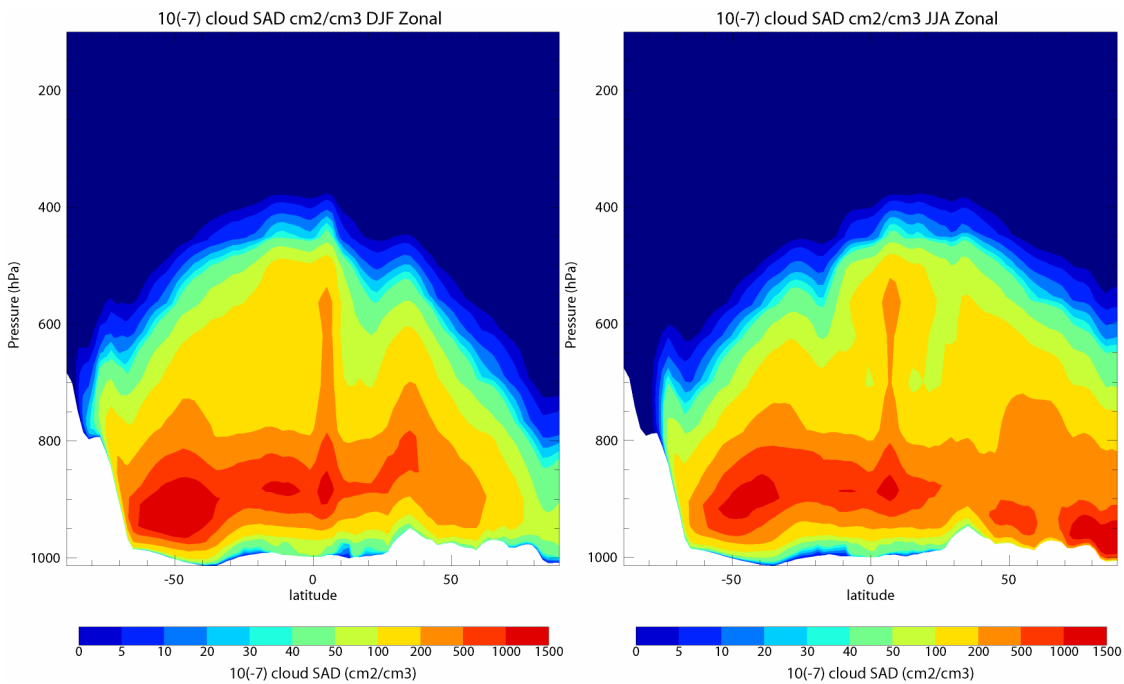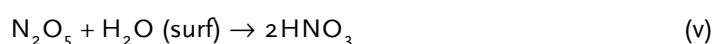
Figure 8: The zonal means of the SAD of cloud droplets for seasons DJF (top) and JJA (bottom) during 2006. The SAD values are much higher than the corresponding seasonal mean SAD values from ice particles as shown in Fig 7, although no SAD from cloud droplets exists in the upper troposphere.

Figure 8 shows the global distribution of SAD from cloud droplets for seasons DJF and JJA. The resulting SAD values in the mid- to lower troposphere are much higher than the corresponding values which occur from ice particles as a result of the larger LWC values and smaller effective droplet radius (not shown), where the maxima occur in the higher latitudes for both hemispheres. Some coverage also exists in the lower troposphere of the tropics, in which no ice particles occur due to the relative high temperatures. In contrast, no significant SAD exists due to cloud droplets above 400hPa, meaning that the reactive surface area in the tropical upper troposphere originates predominantly from ice particles in the model.

# 6. The Effects on the Composition of the Global Troposphere

In terms of the chemical conversion of nitrogen, the effect of updating the calculation of the available SAD is currently limited to the only heterogeneous reaction that is included in the model involving the oxidation of $N_2O_5$ into $HNO_3$ via reaction (v), where the reaction with water is assumed to occur on the surface of the ice/cloud droplet:

$$N_2O_5 + H_2O \text{ (surf)} \rightarrow 2\,HNO_3 \tag{v}$$

In Figs 2 and 3 we have shown that applying Eqns (7) through to (9) results in a significant reduction in the magnitude of KN2O5L in TM4 by a few orders of magnitude throughout the troposphere. When applied online this has the potential to significantly dampen down the global conversion of reactive nitrogen into $HNO_3$, which is the most abundant nitrogen reservoir in the TM model when using the latest chemical updates for the reaction rates (Williams et al, 2009). In this section we analyse the effects of this reduction in the conversion of reactive nitrogen on the composition of the global troposphere and the oxidation potential for trace gas pollutants by using the KHET simulation defined in Table 1.

A further issue concerning the lifetime of $N_2O_5$ is the existence of a gas phase reaction which converts $N_2O_5$ into $HNO_3$ without needing the existence of a reactive surface, reaction (vi), with the rate of this reaction being between 2.0 - 0.25 x $10^{-21}$ molecules$^{-1}$ cm$^3$ s$^{-1}$, independent of either temperature or pressure.

$$N_2O_5 + H_2O \rightarrow 2\,HNO_3 \tag{vi}$$

Although the rate is many orders of magnitude lower than most gas-phase reactions, the process is made more important by the high $[H_2O]_g$ that occurs throughout the troposphere. Recently, Emmerson and Evans (2009) have identified this reaction as being the cause of significant uncertainty between the different reaction chemical mechanisms when compared in a chemical box model. Moreover, the reaction is also included in the original CBM4 reaction mechanism of Gery et al (1989), but was subsequently excluded in the reduction of the mechanism by Houweling et al (1998). Box modeling simulations show that this reaction has a significant effect concerning the partitioning of nitrogen (and thus $O_3$ formation) when comparing the original CBM4 mechanism with the modified CBM4 mechanism (not shown) in the absence of heterogeneous conversion processes. Therefore we also use the final sensitivity test, denoted KNEW in Table 1, in order to assess the compensating effects of applying this reaction online, in tandem with the new parameterizations for $r_{eff}$ and SAD.

## 6.1 Annually integrated zonal differences for $HO_x$, $NO_x$, $O_3$ and associated chemical reservoirs

In this section we briefly show the cumulative effects of both updating the $K_H$ values and applying Eqn (7) online on the distribution of important trace gas species in TM4. Figure 9 shows the zonal differences between the BASE simulation and the KHET simulation for the species $NO_x$, $HO_2$, $HNO_3$, CO, $O_3$ and OH, respectively. Analysis of the chemical budget terms shows that there is a decrease in $[HNO_3]$ formation from Eqn (v) by ~50% as a result of introducing Eqn (9) into the code for the calculation of the conversion rate. This is somewhat moderated by an associated increase in the conversion of $N_2O_5$ on aquated aerosol (similar to that shown in Appendix D for the KNEW simulation) as a result of elevated $[N_2O_5]$ (see later). This also results in a ~10% increase in $[NO_x]$, as shown in Fig 9a. There are associated increases in the production of tropospheric $[O_3]$ resulting in an increase in the tropospheric $O_3$ burden of ~3%. The subsequent

● ● ● ●     17

enhancement in [OH] also results in a reduction in the tropospheric burden of CO by ~6% (~8%) when comparing the KHET simulation against the KHENRY (BASE) simulation, respectively, as well as decreasing the lifetime of $CH_4$ (c.f. Appendix B). For [$HO_2$], the decreases are similar to those shown in Sect. 4 indicating that the effects of updating the $K_H$ values remain largely intact. For TM5, the differences between the corresponding BASE and KHET simulations are likely to be much less considering the more modest change in $KN_2O_5L$ (not shown).



Figure 9: The zonal differences in the annual mean distribution for (a) $NO_x$, (b) $HO_2$, (c) $HNO_3$, (d) CO, (e) $O_3$ and (f) OH. The differences are calculated using (KHET-BASE)/BASE*100.
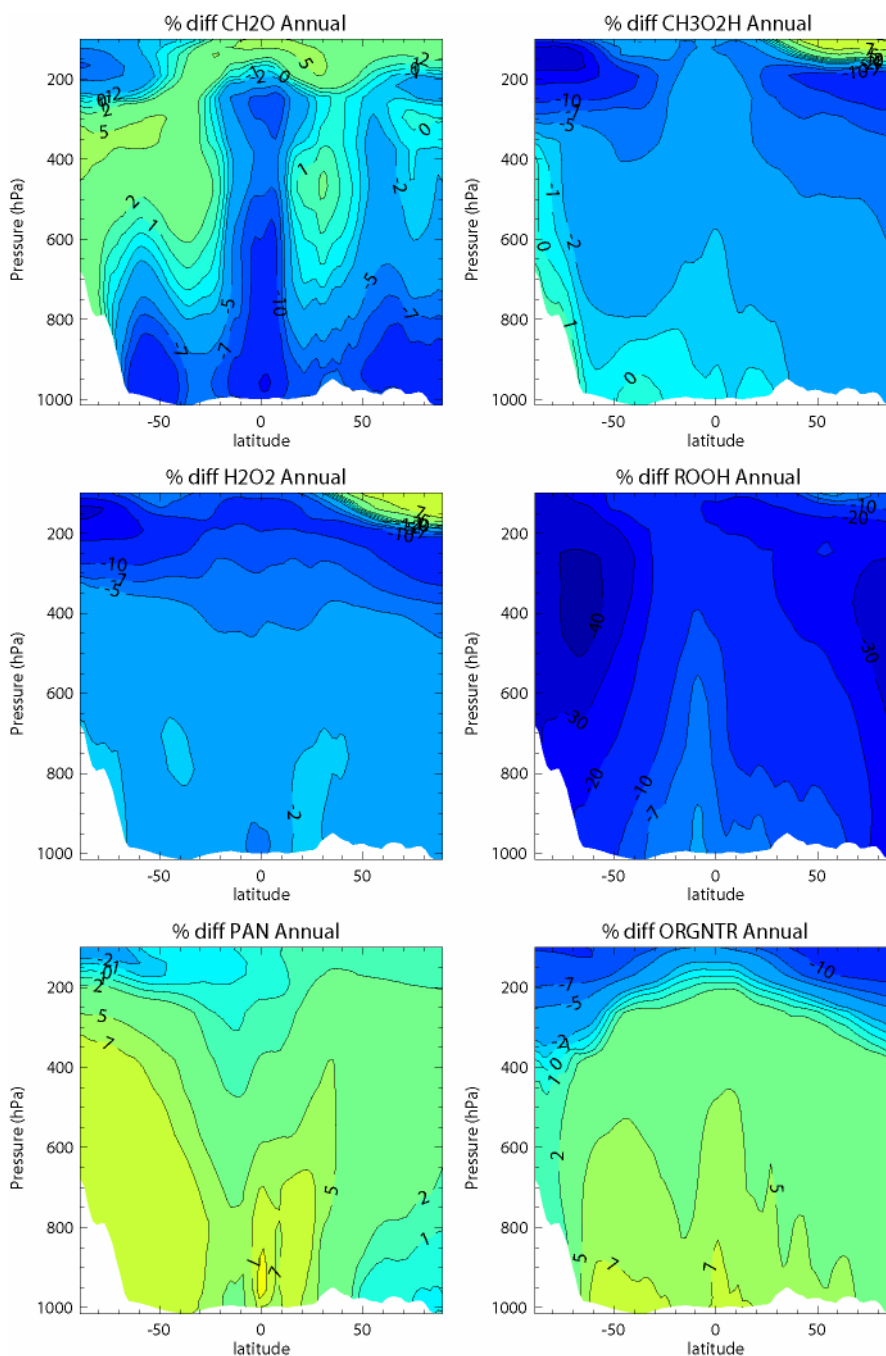
Figure 10: The zonal differences in the annual mean distribution for (a) HCHO, (b) $CH_3O_2H$, (c) $H_2O_2$, (d) ROOH, (e) PAN and (f) ORGNTR for the KHET simulation. The differences are calculated using (KHET-BASE)/BASE*100.

Figure 10 shows the corresponding differences for the main $HO_x$ and $NO_x$ reservoirs included in the modified CBM4 chemical mechanism (Houweling et al, 1998). In general, HCHO, $H_2O_2$ and ROOH all decrease compared to the BASE simulation due to the updates to the $K_H$ values (see Sect 4). The increased formation of both [PAN] and [ORGNTR] occurs as a result of the higher [$NO_x$] and enhance long-range transport of $NO_x$ throughout the troposphere, which subsequently contributes to the increase on [$O_3$] shown in Fig 9e via the release of $NO_2$.
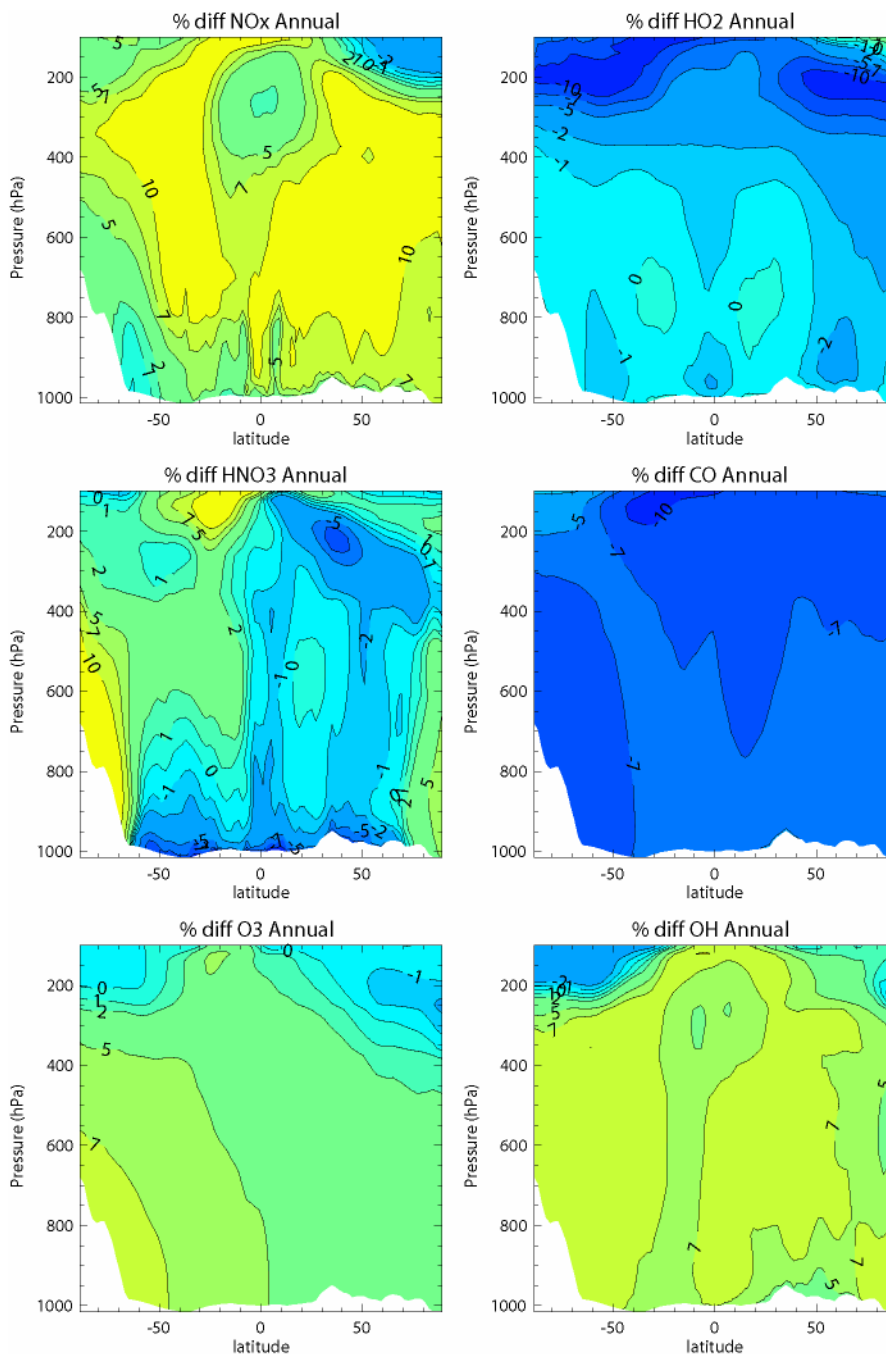
Figure 11: As for Figure 9 except for the KNEW simulation. The differences are calculated using (KNEW-BASE)/BASE*100.

Figure 11 shows the corresponding differences for the KNEW simulation as those shown in Fig 9, where Eqn (vi) is also included in the chemical mechanism. There are strong similarities between the zonal increases of trace species for both KHET and KNEW, except that the KNEW simulation exhibits further increases in tropospheric [$O_3$] of a few percent in the Southern Hemisphere. This subsequently enhances the depletion of [CO], although Appendix 2 shows that the difference introduced into the tropospheric burden is trivial.
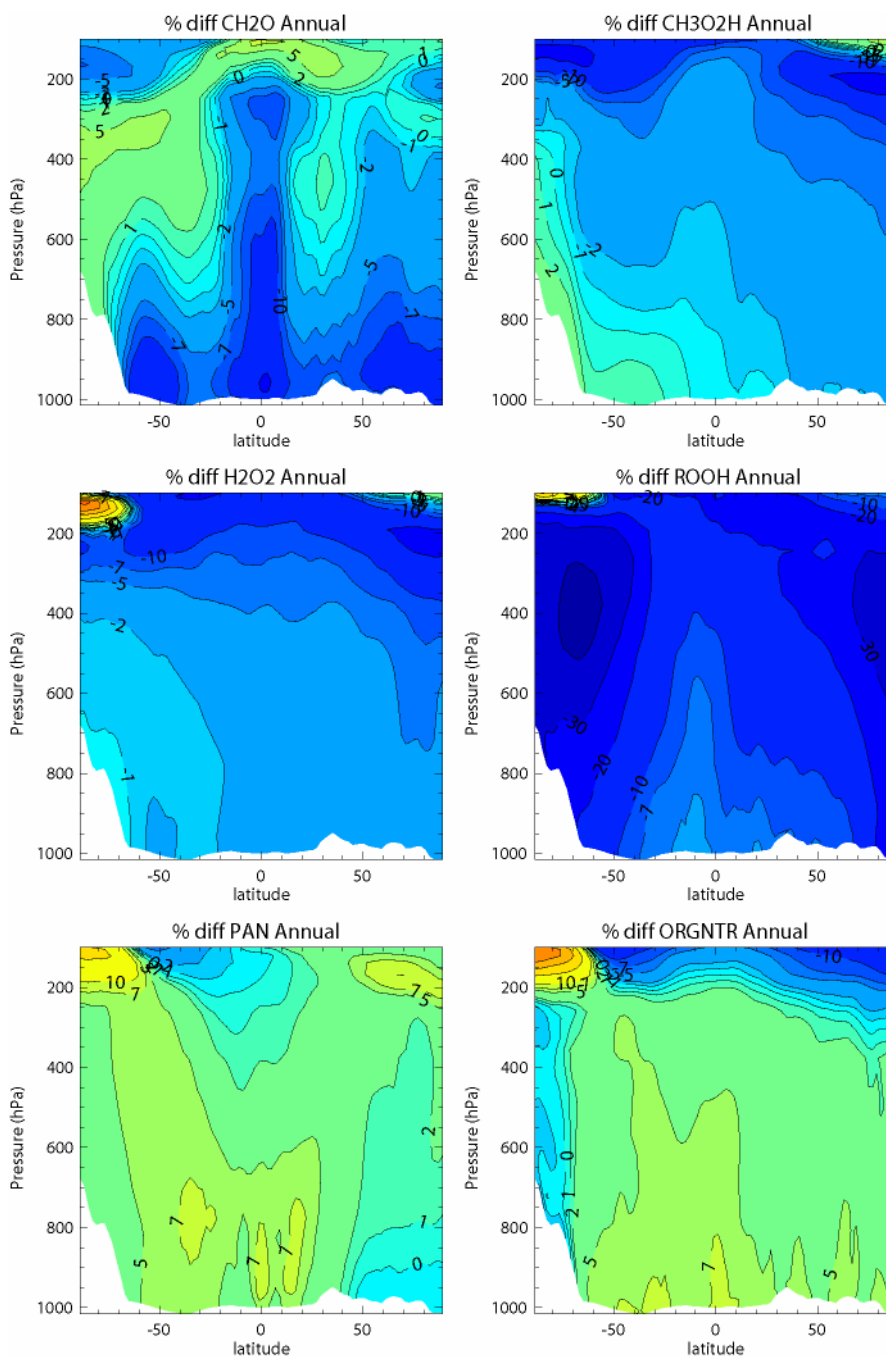
Figure 12: As for Figure 10 except for the KNEW simulation. The differences are calculated using (KNEW-BASE)/BASE*100.

The budget analysis provided for tropospheric $HNO_3$ in Appendix D shows that including the gas phase conversion of $N_2O_5$ does not fully compensate for the lower heterogeneous conversion rate in TM4. Therefore it can be concluded that accounting for the gas phase conversion of $N_2O_5$ does not cause a significant degradation in the performance of TM4. For TM5, where the differences in $KN_2O_5L$ are smaller the application of reaction (vi) could also compensate for the ~50% decrease in the conversion rate.

## 6.2 Annually integrated zonal differences for $NO_3$ and $N_2O_5$

Figure 13 shows the zonal differences in the annual mean for both [$NO_3$] and [$N_2O_5$] between the BASE simulation and the KNEW simulation. It can be seen that there are typically increases ~50-100% throughout large regions of the troposphere for both trace species, although such increases are typically associated with concentrations of a few pptv at most. Due to the efficient photolysis of $NO_3$ during daytime, the maximal differences occur during the night, which is where the largest changes in the rate of oxidation occur. This causes increases in the annual destruction of trace species such as ALD2 (~44%) and ISOP (~20%), although total integrated oxidation by $NO_3$ is typically less important than both OH and $O_3$.
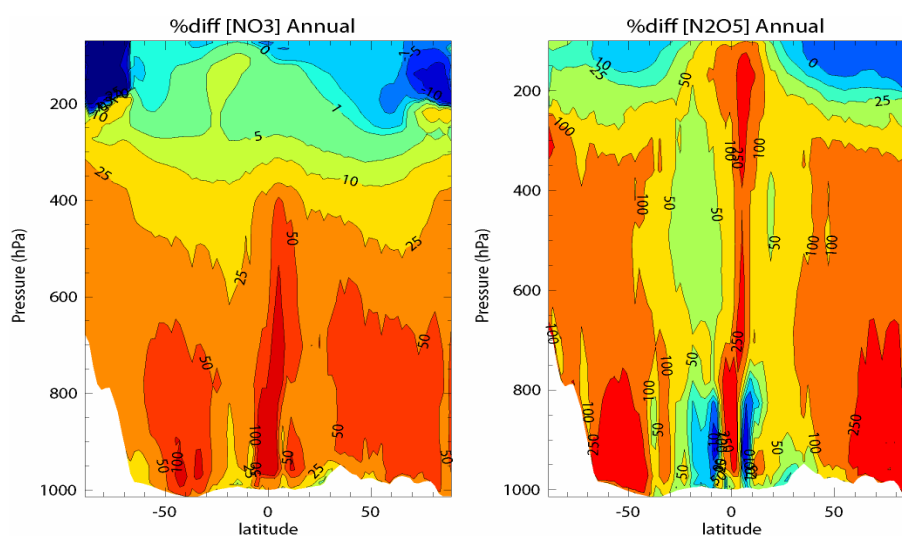


Figure 13: The zonal differences in the annual mean distribution for both (a) $NO_3$ and (b) $N_2O_5$ for the KNEW simulation. The differences are calculated using (KNEW-BASE)/BASE*100.

## 6.3 Comparisons against measurements

Finally, in this section we briefly show some comparisons against a selection of in-situ measurements to gauge whether the updates discussed in the previous sections improves the performance of TM4. To the authors knowledge there are no direct measurements of either $NO_3$ or $N_2O_5$ available during 2006, therefore we choose tropospheric $O_3$ which is both longer lived and measured at numerous locations around the globe by various techniques. In order to examine the effect on the OH budget we also show selected comparisons of CO, which can be used as a diagnostic for the accumulated changes in [OH]. Moreover, there are a small number of measurements of [HCHO] which are also used.

Figure 14 shows a set of comparisons of interpolated model output for the BASE and KNEW simulations against in-situ measurements made by the British BAe146 aircraft during the EU-AMMA intensive measurement campaign conducted during the West African Monsoon period in August. Four separate flights are shown to give an overall impression of the ability of the model to capture the daily variability, where the aircraft was limited to covering the lower troposphere due to the size of the payload. The flights shown occurred on the 6th, 13th, 15th and 17th of August, respectively. In the majority of cases there are large fluctuations in both CO and $O_3$ as the aircraft encounters air-masses which are affected by local emissions and air-masses which have been chemically aged. Many of these fluctuations are not captured by the model, which is not surprising considering that a monthly mean emission source is prescribed for all types of emission source, although a daily burning cycle is imposed on the biomass burning emissions (c.f. Sect 2). Intense rainfall events result in intense spurts of NO from the soil in the region (Stewart et al, 2008) which has a large effect on the formation of tropospheric $O_3$ in the African troposphere (e.g. Delon et al, 2008; Williams et al,

2009). The model has no means of accounting for such dramatic fluctuations resulting in a dampened variability in tropospheric $O_3$ in the African troposphere.
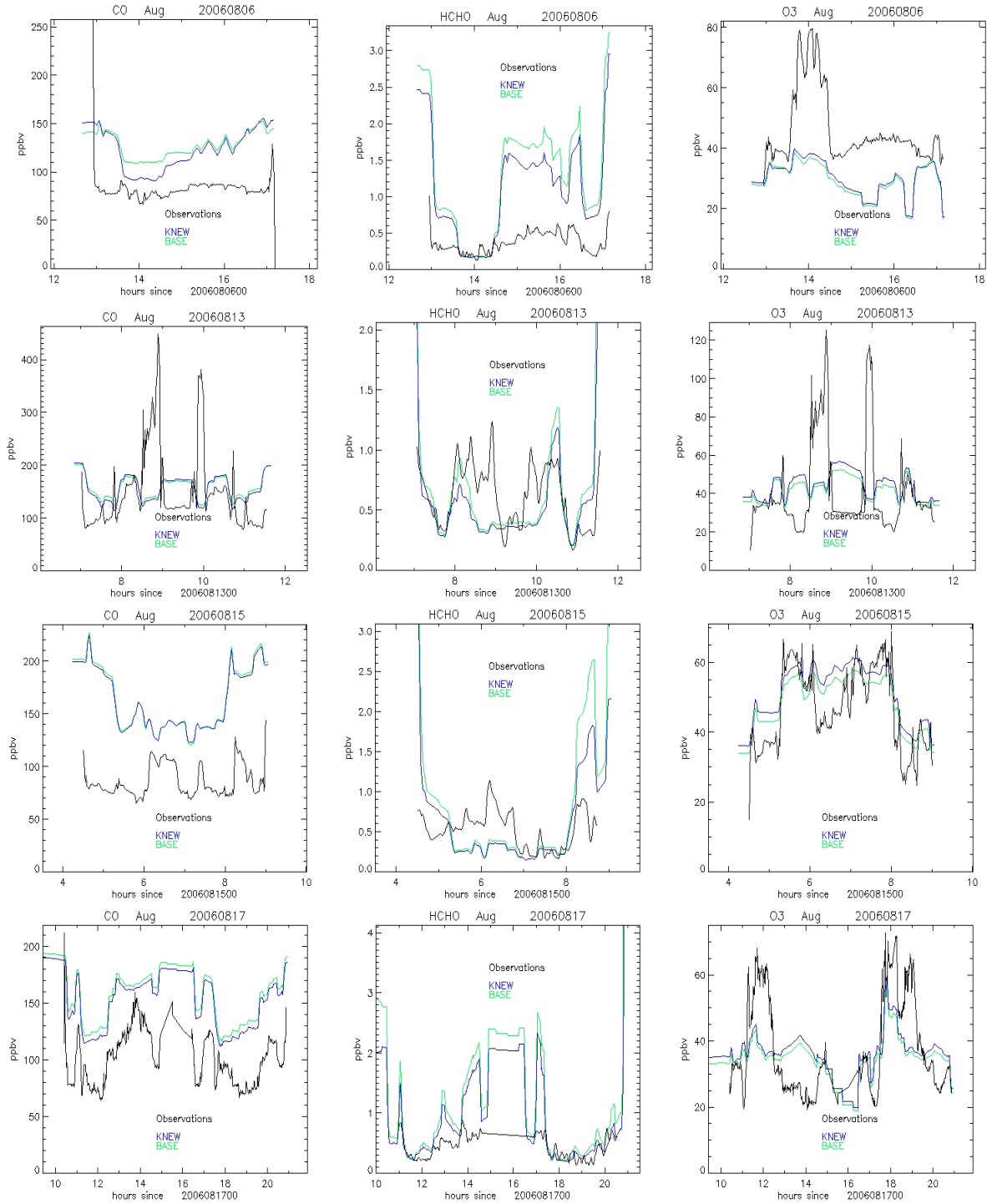


Figure 14: Comparisons of CO, HCHO and $O_3$ between the BASE simulation, KNEW simuation and in-situ observations made by the British BAe 146 Aircraft for four days during August 2006 above Equatorial Africa. The interpolations are performed along the flight trajectories using the method documented in Brunner et al (2003).

In general the model tends to over-estimate tropospheric [CO] at these altitudes by between ~20-50%. Comparing the two simulations shows that, for CO, there is no real improvement as a result of updating the heterogeneous reaction data. For [HCHO] the agreement between the simulations and the measurements is quite varied, although in many instances the model over-estimates [HCHO]. For this species there is a clear improvement from applying the update to the scavenging co-efficients on the performance of the model. For tropospheric $O_3$ the large variability in the measurements over relatively short periods of time is never really captured by the model. Moreover, the difference between simulations appear as an offset (with KNEW being slightly higher than BASE in accordance with Figure 10) meaning that, although the relative agreement may improve for selected periods, there is no real effect on capturing the observed variability. This is to be expected considering that the lack of variability is most likely due to applying a fixed emission for (e.g.) biogenic NO, which has been shown to influence tropospheric $O_3$ in the African troposphere (e.g. Aghedo et al, 2007; Williams et al, 2009).

In Appendix E we compare seasonal means assembled from the BASE and KNEW simulations against the corresponding values calculated using the vertical ozone profile soundings from a number of different measurement stations. Here the seasonal means are constructed using only model output for the identical days upon which each measurement was taken to provide a fair comparison. Figure E1 and E2 shows comparisons for selected mid-latitude stations for seasons DJF and JJA, respectively. For DJF the KNEW simulation gives is a clear improvement in the mid-troposphere, although the model still under-predicts measured values by ~10ppbv for most of the stations shown. However, the magnitude of the improvement is low compared to the 1-σ variability of the seasonal averages. For season JJA a similar behaviour is shown, although the differences between each of the simulations are somewhat larger than for DJF and extend down to the surface. It has been shown that TM4 generally over-estimates surface ozone values compared to seasonal composites from radiosonde data (Williams et al, 2009) therefore increases in these lower layers tend to make the agreement worse for the lower troposphere. Given the relatively homogeneous increase throughout the lower to mid-troposphere, the KNEW simulation again results in a closer agreement with the measurements in the mid-troposphere. For the upper troposphere, the SAD values fall significantly limiting the importance of heterogeneous conversion meaning that the profiles from both simulations generally merge. Moreover, the gas phase $[H_2O]$ is also low meaning that reaction (vi) has a negligible effect. The corresponding profiles for the KHET simulation are nearly identical to those shown for the KNEW simulation.

Figures E3 and E4 show corresponding comparisons for selected tropical stations. In general the agreement between the seasonal means from the model and measurements is worse for these locations, which could be due to the reduced number of measurements used for calculating the seasonal means, the quality of the meteorological data in the tropics which drives the model or the greater influence of long-range transport from other regions which is not captured by the model. For season DJF, the fact that the model fails capture the complicated vertical structure measured at most of the locations masks whether the upgrades made to the heterogeneous reaction data actually improves the performance of the model for these locations. For instance, at Sepang Airport (2.7°N, 101.7°E) there is a marked improvement, whereas for San Cristobel (0.9°S, 89.6°W) the KNEW simulation leads to a larger disagreement. For JJA the results of the comparisons again give rather a mixed picture, where the improvements seen at Paramaribo (5.8°N, 55.2°W) and San Cristobel are not seen for Sepang Airport in contrast to season DJF, although number of measurements used for the Sepang Airport seasonal mean for JJA is very low. A similar picture can be seen in the seasonal means for the three African stations shown in Figure E5. Again, the KHET profiles are nearly identical to those shown for KNEW.

Finally Figure 15 shows comparisons of seasonal averages for both the BASE and KNEW simulations against the MOZAIC in-flight data record taken in the African upper troposphere for all seasons during 2006. This measurement dataset is more statistically robust compared to those which originate from the ozone soundings in that a measurement is taken every 2 days covering a much wider area during both day and night thus capturing diurnal variability. In general, the agreement between 10°S-10°N improves for the KNEW simulation due to TM4 generally under predicting the seasonal average. However, for the second half of the year the agreement becomes worse between 20°S-10°S, with the KNEW seasonal average being too high by ~5-10ppbv. Comparisons using seasonal means from the KHET simulation (not shown) reveal that this disagreement is principally due to the inclusion of the gas phase conversion of $N_2O_5$. This feature cannot be seen in the JJA comparisons using the African ozone sonde stations, although these stations are located away from the latitudinal zone where the largest discrepancy occurs. Moreover, analysis of the chemical budget

terms shows that for the tropical tropopause region between 20°S-20°N for the pressure regimes 250-90hPa the heterogeneous loss terms dominate the loss of $N_2O_5$ as a result of the low $[H_2O]$ at these levels. Therefore, this increase in the seasonal mean for JJA is not fully understood.
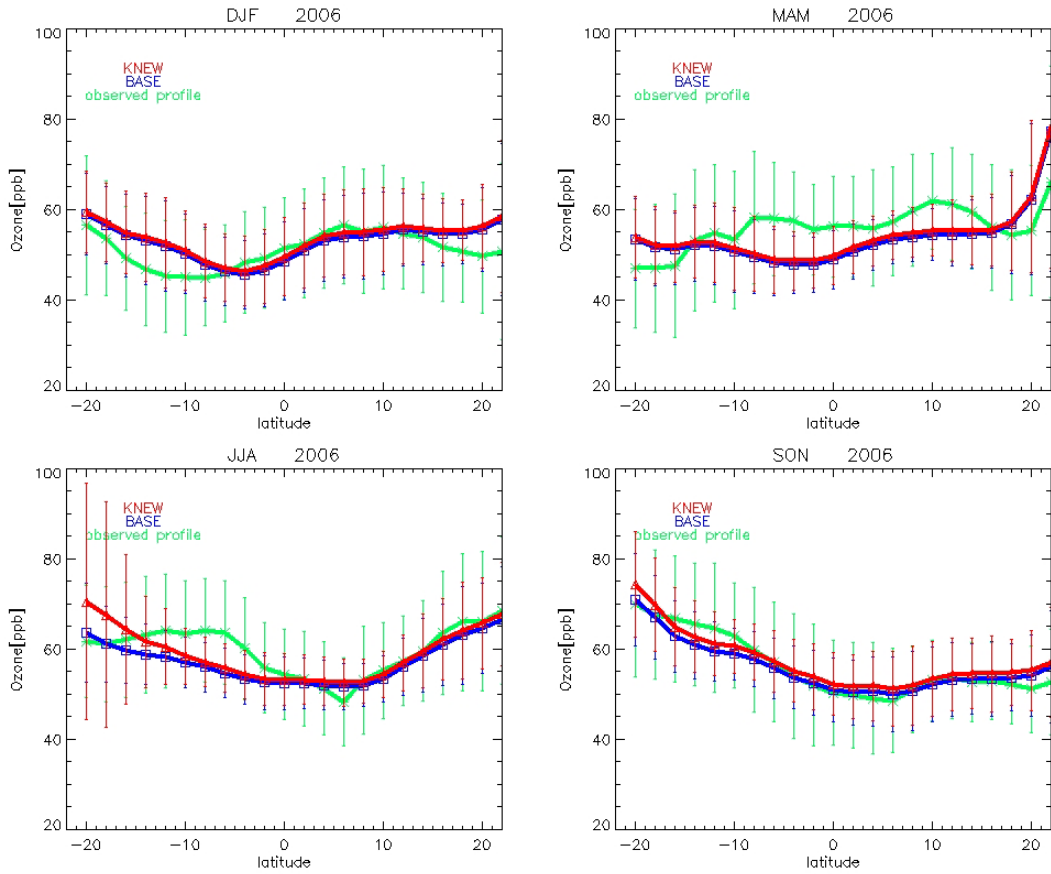


Figure 15: Comparisons of upper tropospheric $O_3$ between the BASE simulation, KNEW simulation and in-situ observations made by the MOZAIC measurement campaign. The interpolations are performed along the flight trajectories using the method documented in Brunner et al (2003).

## 6.3 Further Discussion

Although reaction (vi) is in both the IUPAC and JPL recommendations there is still some ambiguity associated with the rate of the reaction, whether the reaction is bi- or tri-molecular and the atmospheric significance of the reaction in the presence of heterogeneous surfaces. In a recent box model intercomparison study of chemical mechanisms used in CTM's, Emmerson and Evans (2009) concluded that reaction (vi) is a major source of uncertainty which exists between the different chemical mechanisms tested. By comparing the budget terms for $HNO_3$ between the KHET and KNEW simulations (not shown) we can conclude that the inclusion of reaction (iv) in a global CTM containing heterogeneous conversion only increases the total conversion of $N_2O_5$ by <5%. This is due to a compensating effect in which both of the heterogeneous conversion terms are reduced in KNEW due to the limitations associated with the available $[N_2O_5]$. Moreover, the degradation of the model performance in the upper troposphere (Figs 15c and d) does not provide confidence for applying the reaction under meteorological conditions which are far removed from those under which the rate was determined. Further evidence concerning the atmospheric importance of this reaction comes from the *in-situ* measurement study of Brown et al (2007) concerned with $NO_3$ and $N_2O_5$ profiles in the nighttime boundary layer. In the analysis of their results the authors do not deem reaction (iv) to be important enough to warrant discussion, where the conversion is limited to heterogeneous routes only. Therefore, from the findings of this sensitivity study we do not recommend inclusion of reaction (iv) in the modified CBM4 mechanism for use in the TM model.

# 7 Conclusions and recommendations

In this technical report we have shown that updating the heterogeneous reaction data used online in the TM model for the calculation of the uptake of soluble trace gas species into cloud droplets to the latest measurement data results in significantly higher Henry's law co-efficients compared to those in the current version of the TM model. This is, in part, due to the explicit introduction of hydration, which increases the efficiency at which trace species can be removed from the gas phase. When applied online these new uptake values result in a reduction in the global burdens of a number of important $HO_x$ precursors such as HCHO and $H_2O_2$ by between ~3-5% (increasing to between ~5-10% in the tropics). The wet deposition of HCHO increases by ~65% which results in a decrease in $[HO_2]$ by between ~1-2% as a seasonal mean. This subsequently reduces the *in-situ* production of the main peroxy species such as $[CH_3O_2H]$. Moreover, the enhanced scavenging introduced for the peroxy species also contributes in the reduction in the global burdens for each respective species. The two additional Henry's law co-efficients added for $CH_3COCHO$ and ALD2 both result in loss of the trace species via wet deposition, becoming the second most important loss term for $CH_3COCHO$ due to the extent of the hydration once in solution.

For a more accurate description of the micro-physical properties of ice particles we have introduced parameterizations for the derivation of both the effective radius and the surface area density of the ice field present in each model grid cell, which both utilize the Ice Water Content product provided in the ECMWF meteorological data. Comparing the average particle sizes shows that those calculated using the new parameterization are typically smaller than the fixed particle size of 50μM prescribed in previous versions of the TM model. This generally results in a larger total surface area for reactive uptake compared to using a fixed particle size. For cloud droplets the effective radius has been reduced 20%, from 10μM to 8μM, in order to provide consistency throughout the TM model. The calculation of the heterogeneous conversion of $N_2O_5$ has been homogenised between ice particles, cloud droplets and aquated aerosol particles by introducing explicit values for the reactive surface area. For TM4, this leads to a significant reduction in the conversion rate on cloud droplets, which subsequently increases both $[N_2O_5]$ and $[NO_3]$ in the gas phase. This also results in increases in tropospheric $[O_3]$ by a few percent at a global scale. For TM5 the differences are more modest, where reductions in the conversion rate of the order of ~50% occur.

Finally, the gas phase conversion of $N_2O_5$ with water vapour has been introduced into the modified CBM4 mechanism and applied online to determine the influence on tropospheric composition. Comparisons of the resulting zonal annual means of the tracer fields and analysis of the chemical budget shows that the effect of including this reaction is not significant in the presence of heterogeneous reactions involving $N_2O_5$. The application throughout the model domain can result in degradations in model performance for the upper troposphere. Moreover, a certain degree of ambiguity exists regarding the actual rate constant and mechanism associated with this reaction.

In summary, it is recommended that the updated heterogeneous scavenging rates, homogenization of the cloud droplet size and the use of explicit surface area densities for both cloud and ice particles is adopted across all version of the TM model. The inclusion of the gas phase conversion of $N_2O_5$ into $HNO_3$ does not produce significant improvements or chemical effects when applied online meaning that it should not be included in the modified CBM4 mechanism for future chemical studies.
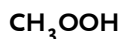
## Acknowledgements

# Appendix A

## Changes in the Global Chemical Budget Terms for Peroxide Species due to Updates to $K_H$

### $H_2O_2$

| Reaction | Global | Southern Hemisphere (90-20°S) | Tropics (20°S-20°N) | Northern Hemisphere (20-90°N) |
|---|---|---|---|---|
| $HO_2 + HO_2 \rightarrow H_2O_2$ | 887.2 (-3.7%) | 127.6 (-3%) | 536.6 (-4.2%) | 223.0 (-2.8%) |
| $OH + H_2O_2 \rightarrow HO_2$ | 214.2 (-2.6%) | 28.5 (-2.3%) | 126.9 (-3%) | 58.8 (-1.9%) |
| $H_2O_2 + h\nu \rightarrow 2OH$ | 240.5 (-3.8%) | 40.2 (-3%) | 137.1 (-4.3%) | 63.2 (-2.9%) |
| Wet Dep | 360.7 (-3.4%) | 50.5 (-3.3%) | 229.3 (-4.6%) | 80.9 (-3.3%) |
| Dry Dep | 69.7 (-4.4%) | 9.6 (-3.7%) | 42.8 (-5.2%) | 17.3 (-3.1%) |

Table A: The global chemical budget of $H_2O_2$ integrated over the year 2006. The values are given in total Tg $H_2O_2$ yr[-1] for the BASE run with the percentage differences introduced by upgrading the heterogeneous reaction data for $K_H$ given in parenthesis. The global burdens for $H_2O_2$ equal 2.37Tg $H_2O_2$ (BASE) and 2.27Tg $H_2O_2$ (KHENRY).

### $CH_3OOH$

| Reaction | Global | Southern Hemisphere (90-20°S) | Tropics (20°S-20°N) | Northern Hemisphere (20-90°N) |
|---|---|---|---|---|
| $CH_3O_2 + HO_2 \rightarrow CH_3O_2H$ | 1030.3 (-) | 183.1 (-) | 628.2 (-) | 219.1 (-) |
| $OH + CH_3O_2H \rightarrow 0.7\ CH_3O_2 + 0.3OH + 0.3HCHO$ | 790.4 (-) | 126.5 (-) | 496.2 (-) | 167.7 (-) |
| $CH_3O_2H + h\nu \rightarrow HCHO + HO_2 + OH$ | 140.6 (+3%) | 61.6 (+3.8%) | 55.7 (+1.8%) | 23.3 (+5.6%) |
| Wet Dep | 62.2 (+31.8) | 8.0 (+25%) | 36.4 (+35%) | 17.8 (+28.3) |
| Dry Dep | 50.1 (-4.2%) | 3.8 (-5.5%) | 35.0 (-4%) | 11.3 (-4.1%) |

Table B: The global chemical budget of $CH_3O_2H$ integrated over the year 2006. The values are given in total Tg $CH_3O_2H$ yr[-1] for both the BASE run with the percentage differences introduced by upgrading the heterogeneous reaction data for $K_H$ given in parenthesis. The global burdens for $H_2O_2$ equal 2.24Tg $CH_3O_2H$ (BASE) and 2.21Tg $CH_3O_2H$ (KHENRY).

**ROOH**

| Reaction | Global | Southern Hemisphere (90-20°S) | Tropics (20°S-20°N) | Northern Hemisphere (20-90°N) |
|---|---|---|---|---|
| $HO_2 + XO_2 \rightarrow ROOH$ | 857.6 (-2.2%) | 67.9 (-2.2%) | 573.9 (-2.3%) | 215.8 (-2%) |
| $HO_2 + XO_2N \rightarrow ROOH$ | 45.9 (-1%) | 3.3 (-) | 29.9 (-1%) | 12.7 (-1%) |
| $HO_2 + C_2O_3 \rightarrow HCHO + XO_2 + HO_2 + 0.79OH + 0.21ROOH$ | 28.8 (-2.4%) | 2.4 (-) | 18.6 (-2.7%) | 7.8 (-2.2%) |
| $OH + ROOH \rightarrow 0.7XO_2 + 0.3OH$ | 576.9 (-4.1%) | 53.5 (-4.1%) | 368.4 (-4.3%) | 155.0 (-3.6%) |
| $ROOH + h\nu \rightarrow OH$ | 140.6 (+3.2%) | 61.6 (+3.7%) | 55.7 (+1.8%) | 23.3 (+5.6%) |
| Wet Dep | 24.3 (+9.7%) | 8.5 (+7.1%) | 9.4 (+13.7%) | 6.4 (+7.0%) |
| Dry Dep | 22.9 (-1%) | 4.8 (-1.1%) | 14.5 (-1.4%) | 3.6 (-0.9%) |

Table C: The global chemical budget of ROOH integrated over the year 2006. The values are given in total Tg ROOH yr$^{-1}$ for both the BASE run with the percentage differences introduced by upgrading the heterogeneous reaction data for $K_H$ given in parenthesis. The global burdens for ROOH equal 3.19Tg ROOH (BASE) and 3.02Tg ROOH (KHENRY).

# Appendix B

## Changes in the Global Chemical Budget Terms for Tropospheric $O_3$, CO and $CH_4$ due to Updates to $K_H$

| Simulation | Chem $O_3$ Prod (Tg $O_3$ yr$^{-1}$) | Chem $O_3$ Dest (Tg $O_3$ yr$^{-1}$) | Dry Deposition (Tg $O_3$ yr$^{-1}$) | Strat-Trop Exchange (Tg $O_3$ yr$^{-1}$) | $\tau_{O_3}$ (days) |
|---|---|---|---|---|---|
| BASE | 4291 | 4123 | 661 | 493 | 23.9 |
| KHENRY | 4260 | 4095 | 658 | 499 | 23.9 |
| KHET | 4500 | 4305 | 688 | 500 | 23.6 |
| KNEW | 4459 | 4295 | 688 | 529 | 23.7 |

Table A: The changes associated with the chemical production, chemical destruction, dry deposition, Stratosphere-Troposphere exchange and tropospheric lifetime for tropospheric ozone as a result of updating the KH values, introducing a new parameterization for the description of cirrus particles and cloud droplets and the gas phase oxidation of $N_2O5$ by $H_2O$ into the TM 3D global Chemistry Transport Model, respectively.

| Simulation | $B_{O_3}$ (Tg $O_3$) | $B_{CO}$ (Tg CO) | $\tau_{CO}$ months |
|---|---|---|---|
| BASE | 313 | 346 | 1.94 |
| KHENRY | 312 | 334 | 1.87 |
| KHET | 323 | 321 | 1.76 |
| KNEW | 323 | 322 | |

Table B: As for Table A except for the changes associated with the burdens of tropospheric ozone and tropospheric CO.

| Simulation | Tropospheric Destruction of $CH_4$ (Tg $CH_4$ yr$^{-1}$) | $\tau_{CH_4}$ (years) | Atmospheric Chemical Lifetime (years) |
|---|---|---|---|
| BASE | 465 | 9.3 | 10.7 |
| KHENRY | 471 | 9.2 | 10.6 |
| KHET | 501 | 8.7 | 9.9 |
| KNEW | 498 | 8.8 | 10.0 |

Table C: As for Table C except for the changes associated with the annual tropospheric destruction rate of $CH_4$, the atmospheric lifetime of $CH_4$ and the atmospheric chemical lifetime.

# Appendix C

## Seasonal differences in Ice and Cloud physical properties for selected global regions
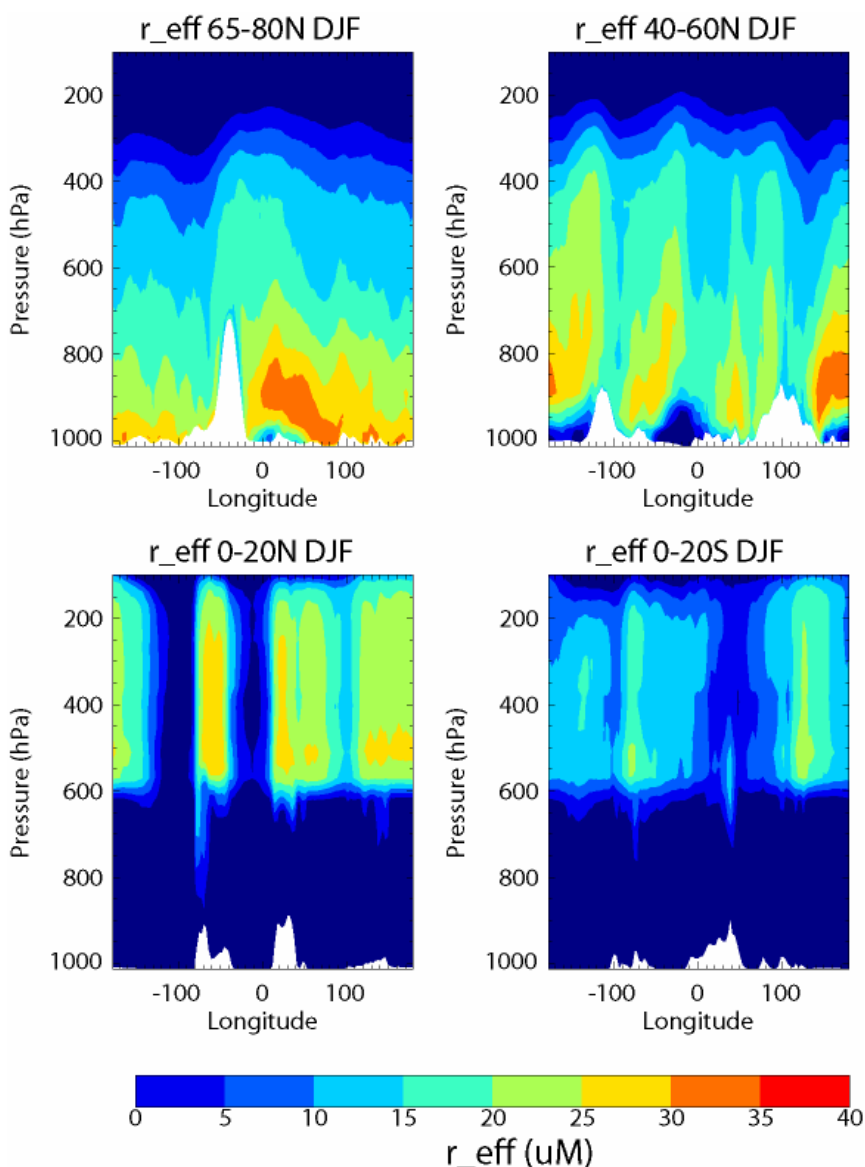


Figure C1: Differences in the effective radii of ice particles as calculated using the ECMWF IWC in Eqn (7) for season DJF during 2006. The longitudinal distribution is shown for 4 different latitudes as denoted in the title of each plot.
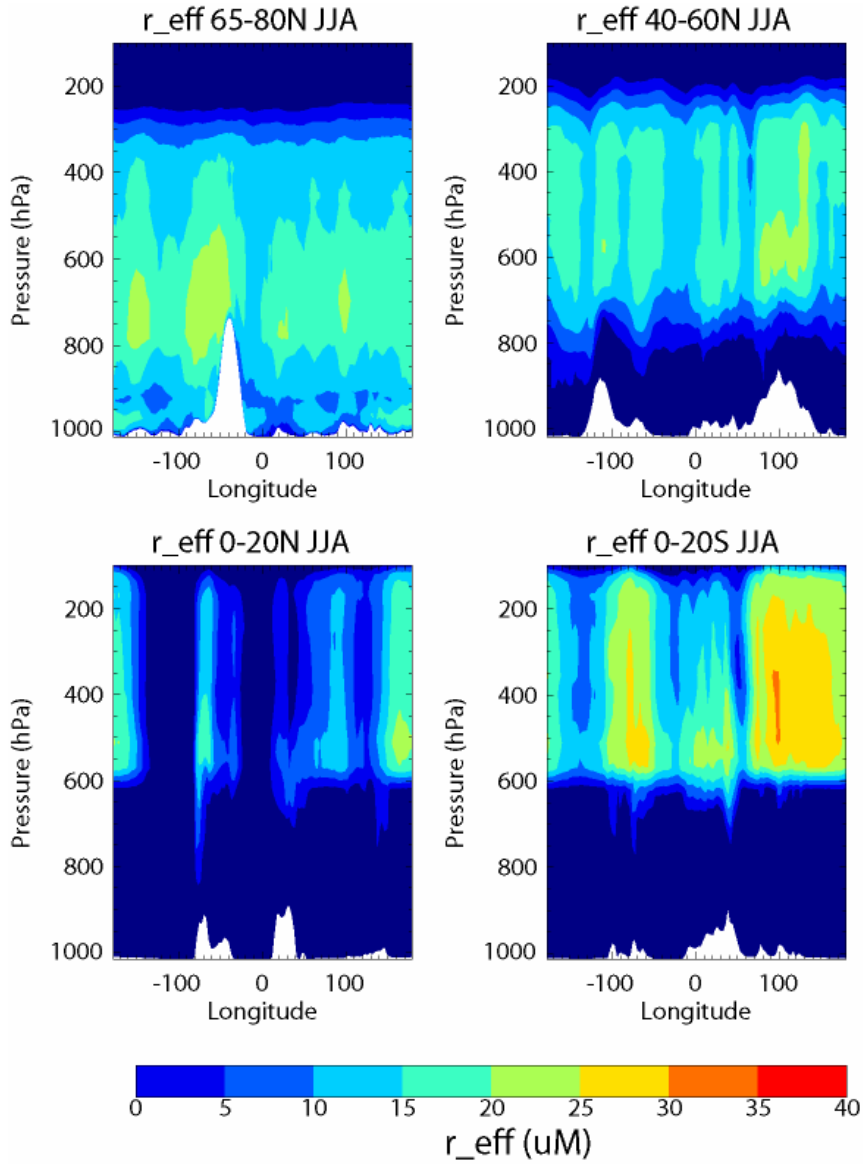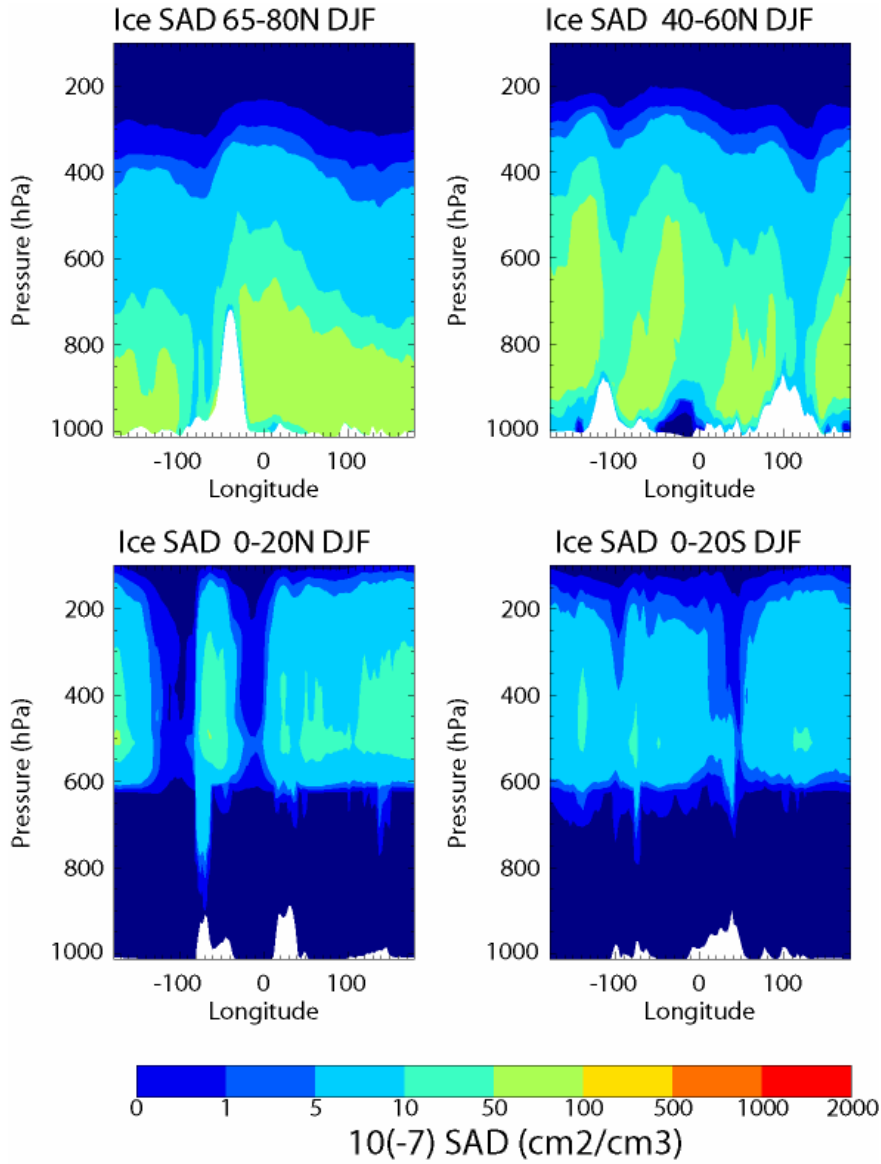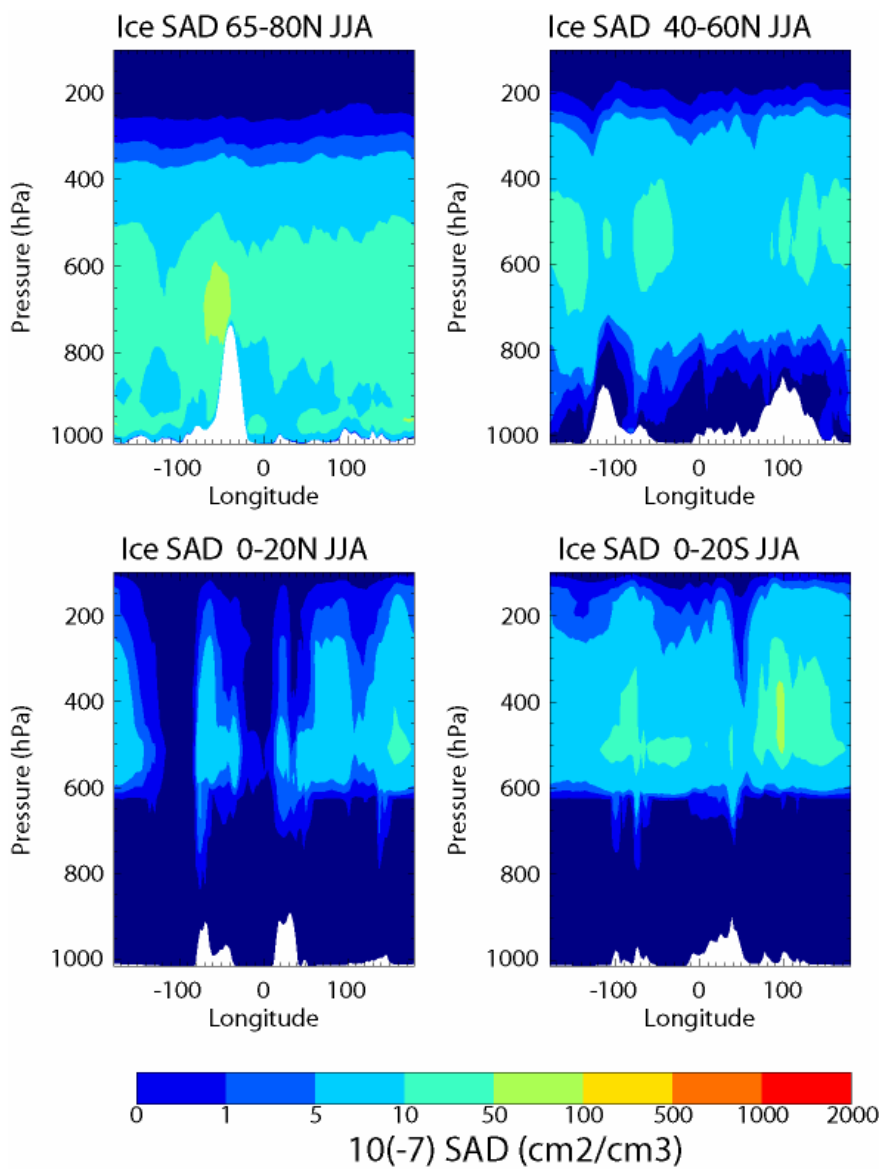
Figure C2: Differences in the effective radii of ice particles as calculated using the ECMWF IWC in Eqn (7) for season DJF during 2006. The longitudinal distribution is shown for 4 different latitudes as denoted in the title of each plot.

Figure C3: Differences in the SAD of ice particles as calculated using the ECMWF IWC in Eqn (6) for season JJA during 2006. The longitudinal distribution is shown for 4 different latitudes as denoted in the title of each plot.

Figure C4: Differences in the effective radii of ice particles as calculated using the ECMWF IWC in Eqn (7) for season JJA during 2006. The longitudinal distribution is shown for 4 different latitudes as denoted in the title of each plot.
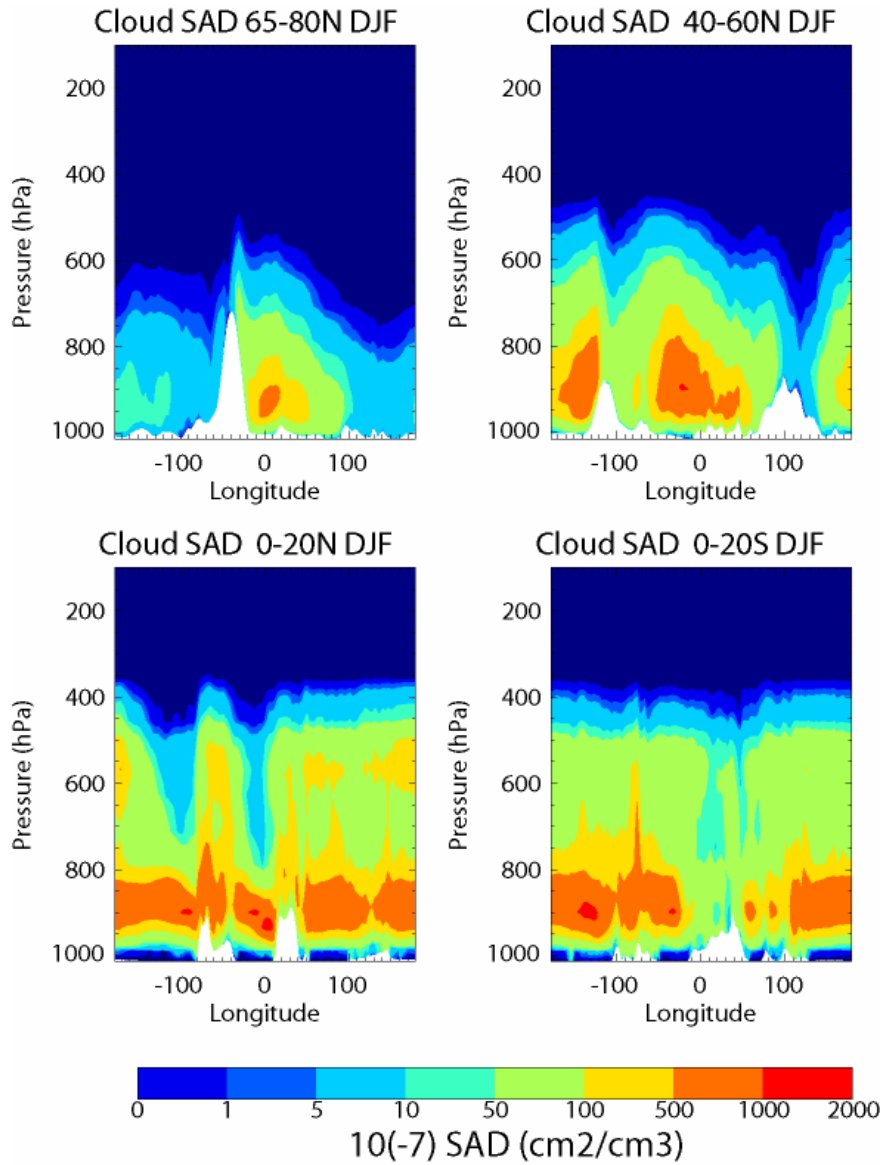
Figure C5: Differences in the SAD of cloud droplets as calculated using the ECMWF LWC for season DJF during 2006. The longitudinal distribution is shown for 4 different latitudes as denoted in the title of each plot.
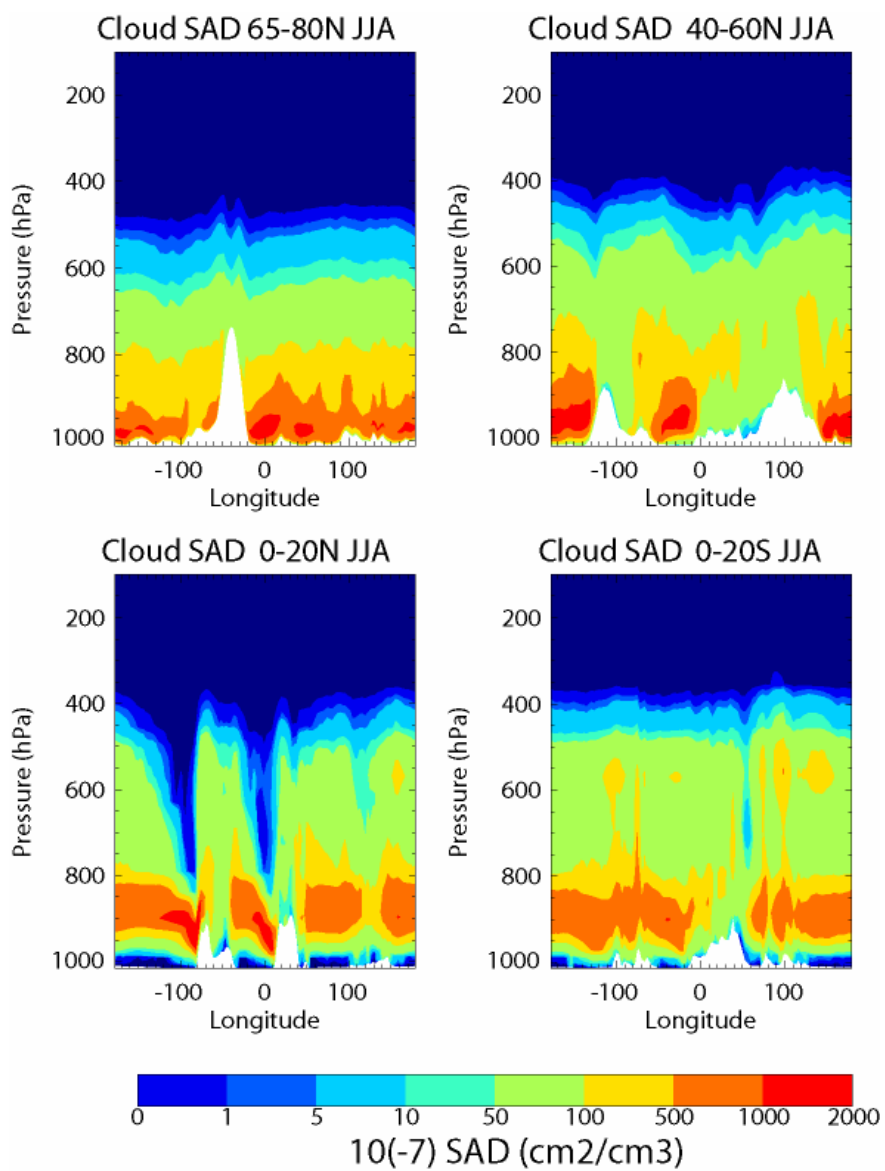
Figure C6: Differences in the SAD of cloud droplets as calculated using the ECMWF LWC for season JJA during 2006. The longitudinal distribution is shown for 4 different latitudes as denoted in the title of each plot.

# Appendix D

## Changes in the Global Chemical Budget Terms for $HNO_3$

| Reaction | Global | Southern Hemisphere (90-20°S) | Tropics (20°S-20°N) | Northern Hemisphere (20-90°N) |
|---|---|---|---|---|
| Production | | | | |
| $OH + NO_2 \rightarrow HNO_3$ | 17.91 (+12%) | 0.44 (+14%) | 11.48 (+12.6%) | 5.99 (+10.1%) |
| $NO_3 + HCHO \rightarrow HNO_3 + CO + HO_2$ | 0.29 (+33%) | 0.00 (+100%) | 0.21 (+29%) | 0.07 (+55%) |
| $NO_3 + ALD2 \rightarrow HNO_3 + C_2O_3$ | 0.65 (+37%) | 0.00 (+55%) | 0.43 (+34%) | 0.21 (+45%) |
| $N_2O_5 + aq \rightarrow 2HNO_3$ | 2.38 (+80%) | 0.02 (+5%) | 0.85 (+47%) | 1.51 (+99%) |
| $N_2O_5 + L \rightarrow 2HNO_3$ | 15.08 (-46%) | 0.27 (-32%) | 7.02 (-49%) | 7.79 (-44%) |
| $N_2O_5 + H_2O \rightarrow 2HNO_3$ | N/A (1.89) | N/A (0.03) | N/A (0.96) | N/A (0.90) |
| | | | | |
| Destruction | | | | |
| $OH + HNO_3 \rightarrow NO_3$ | 1.9 (+6%) | 0.07 (+8%) | 1.73 (+7%) | 0.57 (+5%) |
| $HNO_3 + h\nu \rightarrow OH + NO_2$ | 2.34 (-) | 0.07 (-) | 1.41 (-) | 0.43 (-) |
| Dry Deposition | 9.92 (-3%) | 0.13 (-8%) | 5.67 (-2%) | 4.12 (-4%) |
| Wet deposition | 22.76 (-3%) | 0.99 (-) | 11.42 (-3%) | 10.35 (-2%) |

Table D: The global chemical budget of $HNO_3$ integrated over the year 2006. The values are given in total Tg N yr$^{-1}$ for the BASE run, along with the percentage differences when the terms are compared with the KNEW simulation. For the additional reaction of $N_2O_5$ with $H_2O$, the production term is given for the KNEW simulation only. The global burdens for $HNO_3$ are equal to 0.2168 Tg N (BASE) and 0.2134 Tg N (KNEW), which is a reduction of only ~2%.

# Appendix E

## Comparisons of tropospheric O3 profiles against radiosonde measurements for 2006
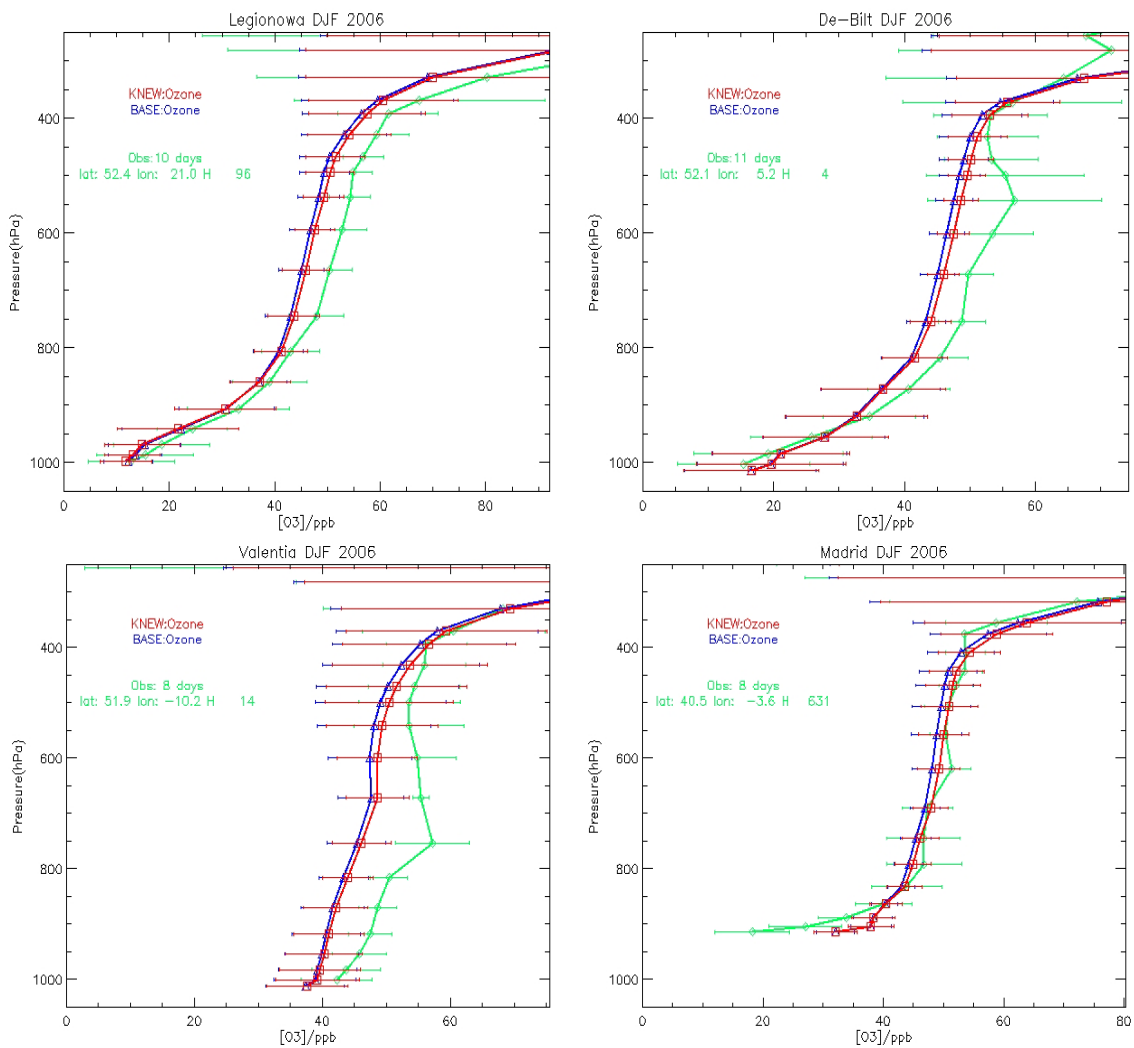
### Mid-latitudes: DJF



Figure E 1: Comparisons of seasonal means of the vertical profiles of tropospheric [O$_3$] for DJF at mid-latitude locations. Seasonal profiles are shown for the BASE simulation, the KNEW simulation and the ozone soundings (green). The details concerning the locations of each sounding station, the number of observations used for each seasonal mean and the height (m) above sea-level are provided within each of the particular diagrams.
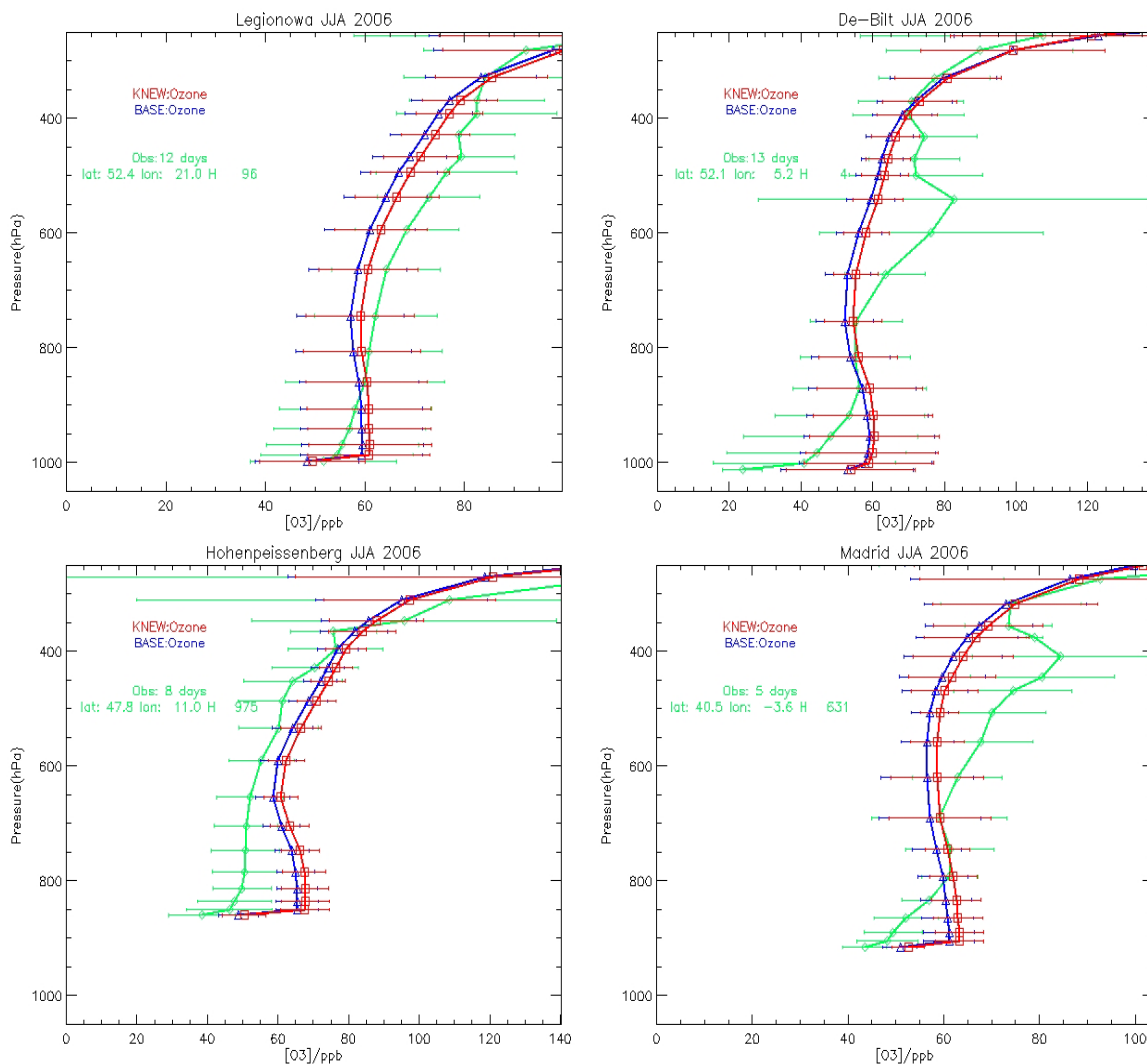
## Mid-latitudes: JJA



Figure E2: Comparisons of seasonal means of the vertical profiles of tropospheric [O$_3$] for JJA at mid-latitude locations. Seasonal profiles are shown for the BASE simulation, the KNEW simulation and the ozone soundings (green). The details concerning the locations of each sounding station, the number of observations used for each seasonal mean and the height (m) above sea-level are provided within each of the particular diagrams.
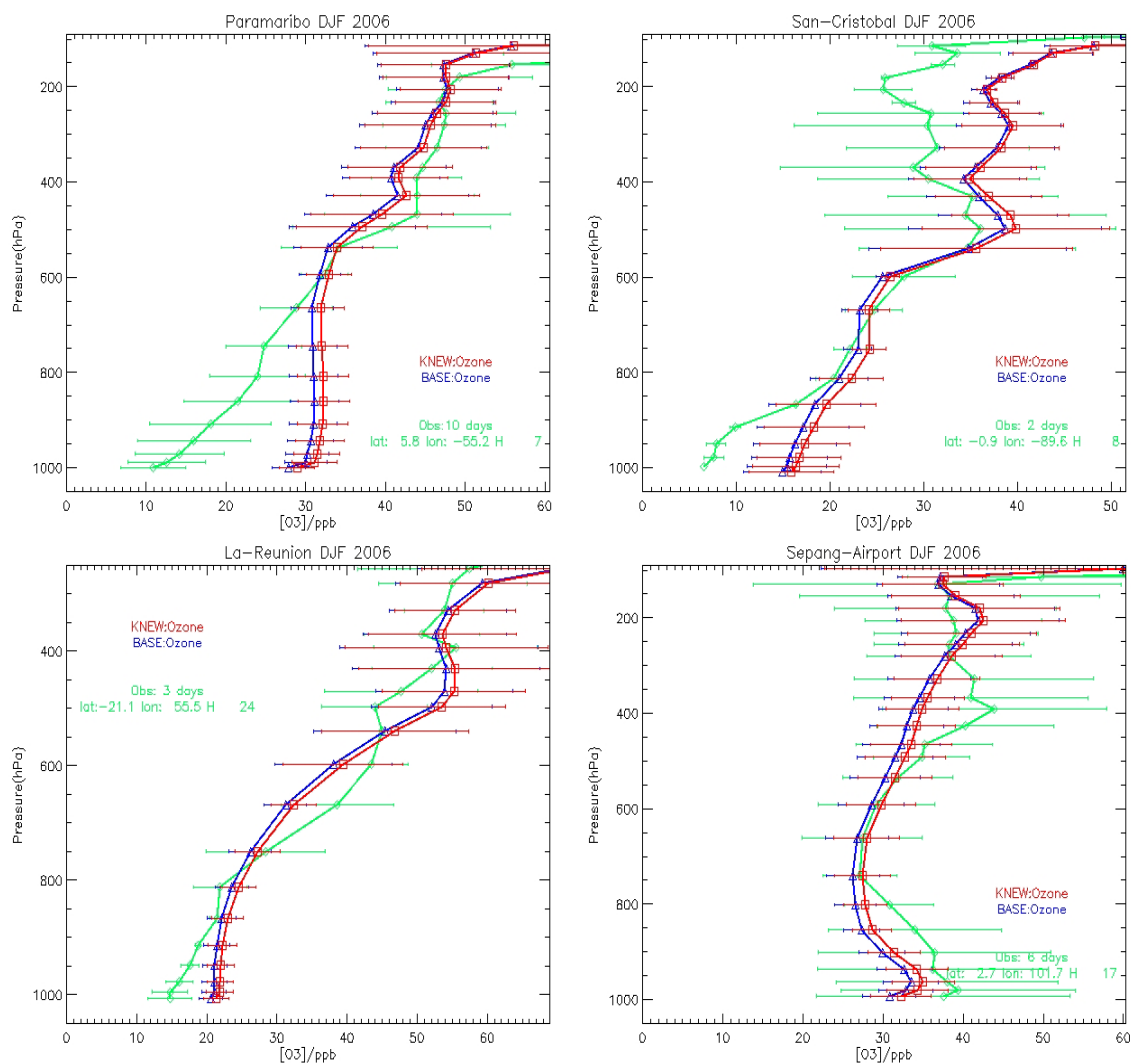
## Tropics: DJF



Figure E3: Comparisons of seasonal means of the vertical profiles of tropospheric [O$_3$] for DJF at tropical locations in the SHADOZ network (Thompson et al, 2003). Seasonal profiles are shown for the BASE simulation, the KNEW simulation and the ozone soundings (green). The details concerning the locations of each sounding station, the number of observations used for each seasonal mean and the height (m) above sea-level are provided within each of the particular diagrams.
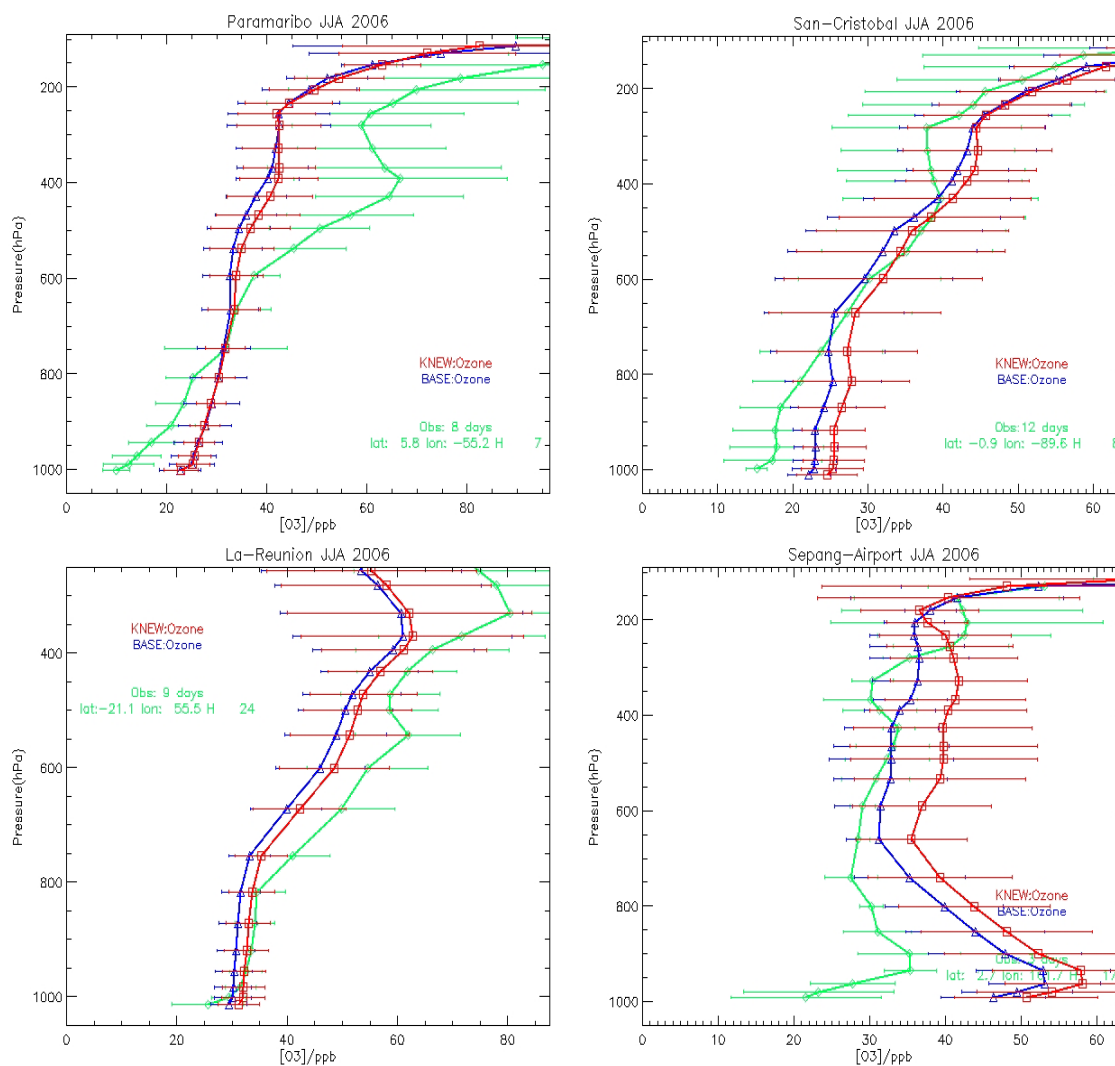
## Tropics: JJA



Figure E4: Comparisons of seasonal means of the vertical profiles of tropospheric [O$_3$] for JJA at tropical locations in the SHADOZ network (Thompson et al, 2003). Seasonal profiles are shown for the BASE simulation, the KNEW simulation and the ozone soundings (green). The details concerning the locations of each sounding station, the number of observations used for each seasonal mean and the height (m) above sea-level are provided within each of the particular diagrams.

## Africa: DJF



Figure E5: Comparisons of seasonal means of the vertical profiles of tropospheric [O$_3$] for DLF for locations in Africa. Seasonal profiles are shown for the BASE simulation, the KNEW simulation and the ozone soundings (green). The details concerning the locations of each sounding station, the number of observations used for each seasonal mean and the height (m) above sea-level are provided within each of the particular diagrams.
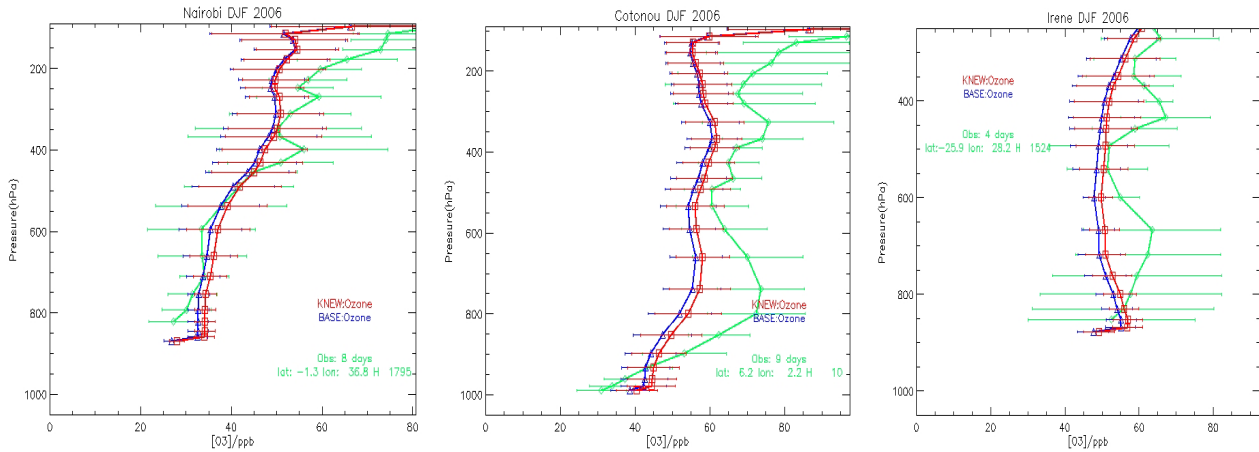
## Africa: JJA



Figure E6: Comparisons of seasonal means of the vertical profiles of tropospheric [O$_3$] for JJA for locations in Africa. Seasonal profiles are shown for the BASE simulation, the KNEW simulation and the ozone soundings (green). The details concerning the locations of each sounding station, the number of observations used for each seasonal mean and the height (m) above sea-level are provided within each of the particular diagrams.
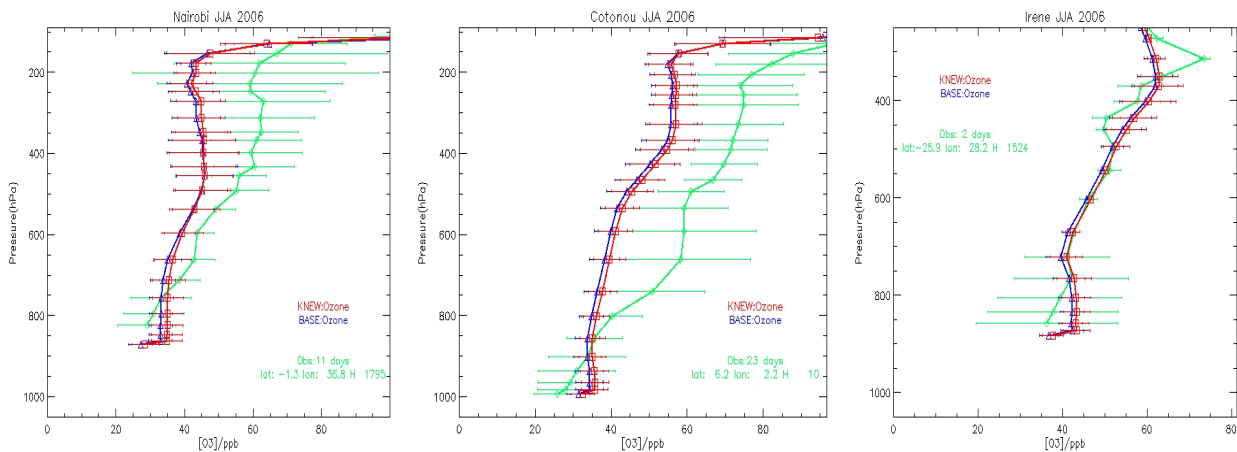
# Bibliography

Aghedo, A. M., Schultz, M. G. and Rast, S.: The influence of African air pollution on regional and global tropospheric ozone, Atms. Chem. Phys., 7, 1193-1212, 2007.

Andres, R. J., and Kasgnoc, A.D., A time-averaged inventory of subaerial volcanic sulfur emissions, *J. Geophys. Res.*, 103, 25251-25261, 1998.

Bertram, T. H., and Thornton, J. A., Toward a general parameterization of N2O5 reactivity on aqueous particles: the competing effects of particle liquid water, nitrate and chlorine, A*tms. Chem. Phys. Discuss.*, 9, 15181-15214, 2009.

Betterton, E. A., and Hoffman, M. R., Henry's law constants of some environmentally important aldehydes, *Environ. Sci. Technol.*, 22, 1415-1418, 1988.

Boersma K. F., Jacob, D. J., Eskes, H. J., Pinder, R. W., Wang, J., and van der A, R. J., Intercomparison of SCIAMACHY and OMI tropospheric NO2 columns: Observing the diurnal evolution of chemistry and emissions from space, J. Geophys. Res., 113, D16S26, doi:10.1029/2007JD008816.

Brown, S. S., Dube, W. P., Osthoff, H. D., Wolfe, D. E., Angevine, W. M., and Ravishankara, A. R., High resolution vertical distributions of $NO_3$ and $N_2O_5$ through the noctural boundary layer, A*tms. Chem. Phys.*, 7, 139-149, 2007.

Brunner, D., Staehelin, J., Rogers, H. L., Köhler, Pyle, J. A., Hauglustaine, D., Jourdain, J., Berntsen, T. K., Gauss, M., Isaksen, I. S. A., Meijer, E., van Velthoven, P. F. J., Pitari, G., Mancini, E., Grewe, V. abd Sausen, R., An evaluation of the performance of chemistry transport models with research aircraft observations. Part 1: Concepts and overall model performance, *Atms.Chem.Phys.*, 3, 1609-1631, 2003.

Delon, C., Reeves, C. E., Stewart, D. J., Serça, D., Dupont, R., Mari, C., Chaboureau, J-P., and Tulet, P., Biogenic nitrogen oxide emissions from soils – impact on $NO_x$ and ozone over West Africa during AMMA (African Monsoon Multidisciplinary Experiment): modeling study, *Atms. Chem. Phys.*, 8, 2351-2363, 2008.

Dentener, F.J, Williams, J.E. and Metzer, S., Aqueous Phase Reaction of HNO4: The Impact on Tropospheric Chemistry, *J. Atms. Chem., 41*, 109-134, 2002.

Endresen, O., Sorgard, E., Sundet, J.K., Dalsoren, S. B., Isaksen, I. S. A., Berglen, T. F., and Gravir, G., Emission from international sea transportation and environmental impact, *J. Geophys. Res.*, 108(D17), doi:10.1029/2002JD002898, 2003.

Emmerson, K. M., and Evans, M. J., Comparison of tropospheric gas-phase chemistry schemes for use within global models, *Atms. Chem. Phys.*, 9, 1831-1845, 2009.

Ervens, B., George, C., Williams, J. E., Buxton, G. V., Salmon, G. A., Bydder, M., Wilkinson, F., Dentener, F., Mirabel, P., Wolke, R., and Herrmann, H., CAPRAM 2.4 (MODAC mechanism): AN extended and condensed tropospheric aqueous phase mechansism and its application, *J.Geophys.Res.*, 108(D14), doi: 10.1029/2002JD002202, 2003.

Fortuin, J.P.F., and Kelder, H., An ozone climatology based on ozonesonde and satellite measurements, *J. Geophys. Res.*, 103(D24), 31709-31734, 1998.

Fu., Q., An accurate parameterization of the solar radiative properties of currus clouds for climate models, *J. Climate*, 9, 2058-2082, 1996.
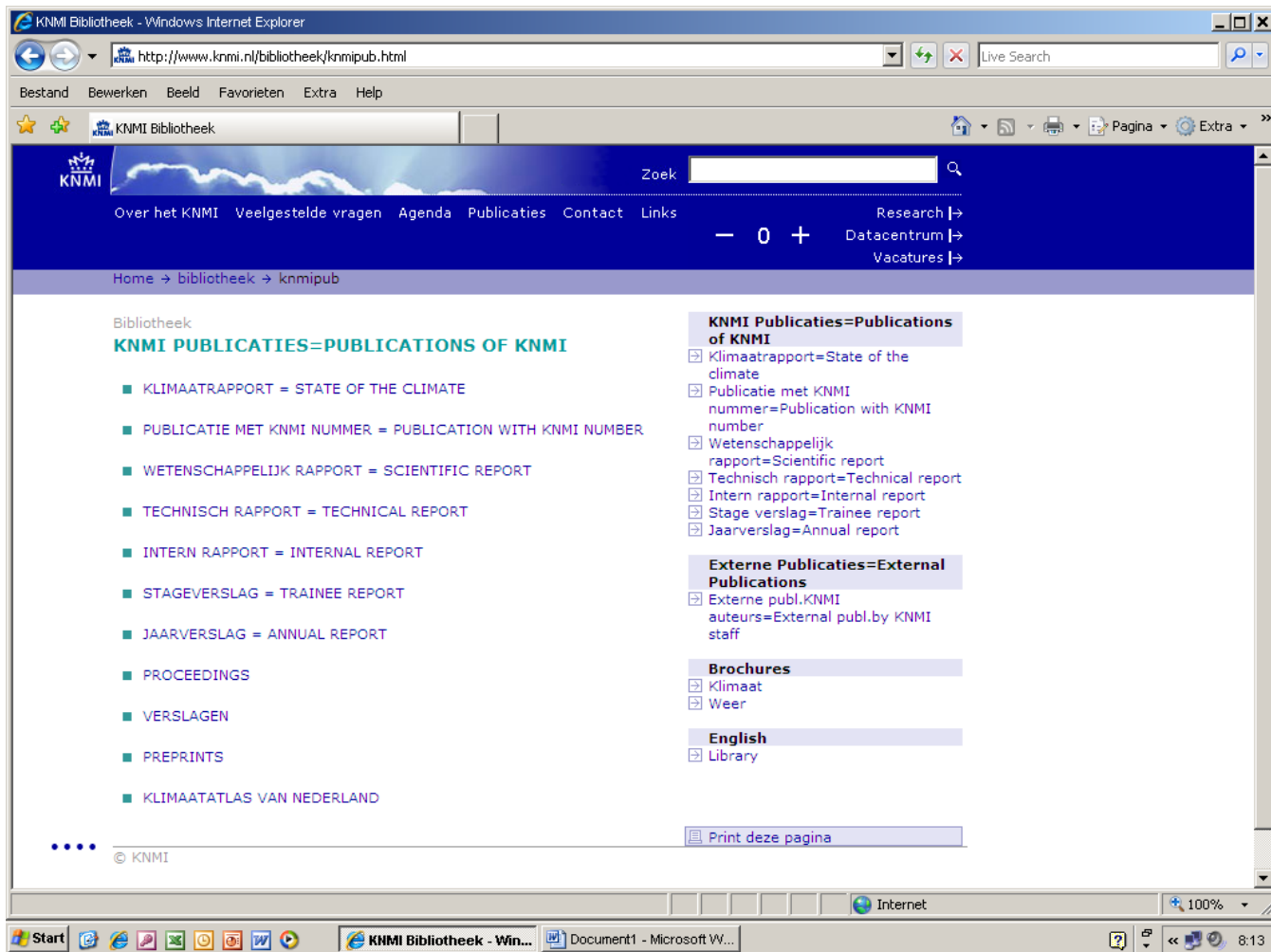
Gery, M., Whitten G. Z., Killus, J. P., and Dodge, M. C., A photochemical kinetics mechanism for urban and regional scale computer modeling, *J.Geophys.Res.*, 94, 18925-18956, 1989.

Grewe, V., Dameris, M., Fichter, C., and Sausen, R., Impact of aircraft NOx emissions. Part 1: Interactively coupled climate-chemistry simulations and sensitivies to climate-chemistry feedback, lightening and model resolution, *Meteorologische Zeitschrift*, 11(3), 139ff, 2002.

Herrmann, H., Tilgner, A.; Barzaghi, P., Majdik, Z., Gligorovski, S, Poulain, L. and Monod, A., Towards a more detailed description of tropospheric aqueous phase organic chemistry: CAPRAM 3.0, *Atms. Environ., 39(23-24)*, 4351-4363, 2005.

Heymsfield, A. J. and McFarquhar, G. M., High albedos of cirrus in the tropical pacific warm pool: Microphysical interpretations from CEPEX and from Kwajalein, Marshall Islands, *J. Atmos. Sci., 53*, 2424-2451, 1996.

Heymsfield, A. J., Properties of Tropical and Midlatitude Ice Cloud Particle Ensembles. Part II: Applications for Mesoscale and Climate Models, *J. Atmos. Sci., 60*, 2592-2611, 2003.

Jacob, D.J., Heterogeneous chemistry and tropospheric ozone, *Atms. Environ.*, 34, 2131-2159, 2000.

Labonne, M., F-M Breon and F. Chevallier, Injection height of biomass burning aerosols as seen from a spaceborne lidar, *Geophys. Res. Letts.*, 34, doi: 10.1029/2007GL029311, 2007.

Lathiére, J., Hauglustaine, D. A., Friend, A. D., De Noblet-Ducoudré, N., Viovy, N., and Folberth, G. A., Impact of climate variability and land use changes on global biogenic volatile organic compound emissions, *Atms. Chem. Phys.*, 6, 2129-2146, 2006.

Lavoué, D., Liousse, C., Cachier, H., Stocks, B. J. and Goldammer, J. G., Modeling of carbonaceous particles emitted by boreal and temperate wildfires at northern midlatitudes, *J. Geophys. Res.*, 105, 26871-26890, 2000.

Lawrence, M. G., and Crutzen, P. J., The impact of cloud particle gravitational settling on soluble trace gas distributions, *Tellus*, 50B, 263-289, 1998.

Liang, J., and Jacob, D. J., Effect of aqueous phase cloud chemistry on tropospheric ozone, *J.Geophys.Res., 102(D5)*, 5993-6001, 1997.

Lind, J. A., and Kok, G. L., Correction to "Henry's law determinations for aqueous solution of hydrogen peroxide, methylhydroperoxide, and peroxyacetic acid" by John A Lind and Gregory L. Kok, *J. Geophys. Res.*, 99D, 21119, 1994.

Lee, D. S., Brunner, D., Döpelheuer, A., Falk, R.S., Ardner, R. M., Lecht, M., Leech, M., Lister, D. L., and Newton, P.J., Aviation emissions present-day and future, *Meteorologische Zeitschrift*, 11 (3), 141-150, 2002

Lelieveld, J. and Crutzen, P. J., Influences of cloud photochemical processes on tropospheric ozone, Nature, 343, 227-232, 1990.

Muller, J. F., Geographical distribution and seasonal variation of surface emissions and deposition velocities of atmospheric trace gases, *J. Geophys. Res.*, 97, 3787-3804, 1992.

O'Sullivan, D. W., Lee, M., Noone, B. C., and Heikes, B. G., Henrys law constant determinations for hydrogen peroxide, methyl hydroperoxide, hydroxymethyl hydroperoxide, ethyl hydroperoxide and peroxyacetic acid, *J. Phys. Chem., 100*, 3241-3247, 1996.

Popp, P.J., Gao, R.S., Marcy, T.P., Fahey, D.W., Hudson, P.K., Thompson, T.L., Kärcher, B., Ridley, B.A., Weinheimer, A.J., Knapp, D.J., Montzka, D.D., Baumgardner, D., Garrett, T.J., Weinstock, E.M., Smith, J.B., Sayres, D.S., Pittmann, J. V., Dhaniyala, S., Bui, T.P., and Mahoney, M., Nitric Acid Uptake on Subtropical Cirrus Cloud Particles, *J. Geophys.Res.,* 109, D06, doi: 10.1029/2003JD004255, 2004.

Roberts, G., Wooster, M. J., and Lagoudakis, E., Annual and diurnal biomass burning temporal dynamics, *Biogeosciences*, 6, 849-866, 2009.

Roelofs, G-J and Lelieveld, J, Distribution and budget of $O_3$ in the troposphere calculated with a chemistry general circulation model, *J. Geophys. Res., 100*(D10), 20983-20998, 1995.

Sander, R. (1999), Compilation of Henry's Law Constants for Inorganic and Organic Species of Potential Importance in Environmental Chemistry (Version 3), (http://www.mpch-mainz.mpg.de/~sander/res/henry.html)

Schmitt, C. G., and Heymsfield, A.J., Total Surface Area Estimates for Individual Ice Particles and Particle Populations, *J.Appl.Meteo.*, 44, 467-474, 2005.

Schumann, U., and Huntrieser, H.: The global lightening-induced nitrogen oxides source, *Atms. Chem. Phys.*, 7, 3823-3907, 2007.

Schwartz, S., Mass transport considerations pertinent to aqueous reactions of gases in liquid water clouds, in *Chemistry of Multiphase Atmospheric Systems, NATO ASI ser.*, vol 6, edited by W. Jaeschke, 415-471, Springer-Verlag, New York, 1986.

Stewart, D. J., Taylor, C. M., Reeves, C. E., and McQuaid, J. B., Biogenic nitrogen oxide emissions from soils: impact of NOx and ozone over west Africa during AMMA (African Monsoon Multidisciplinary Analysis): observational study, *Atms. Chem. Phys.*, 8, 2285-2297, 2008.

Stevenson, D. S., Dentener, F. J., Schultz, M. G., Ellingsen, K., van Noije, T. P. C., Wild, O., Zeng, G., Amann, M., Atherton, C. S., Bell, N., Bergmann, D. J., Bey, I., Butler, T., Cofala, J., Collins, W. J., Derwent, R. J., Doherty, R. M., Drevet, J., Eskes, H. J., Fiore, A. M., Gauss, M., Hauglustaine, D. A., Horowitz, L. W., Isaksen, I. S. A., Krol, M. C., Lamarque, J-F, Lawrence, M. G., Montanaro, V., Müller, J-F, Pitari, G., Prather, M. J., Pyle, J. A. , Rast, S., Rodriguez, J. M., Sanderson, M. G., Savage, N. H., Shindell, D. T., Strahan, S. E., Sudo, K. and Szopa, S., Multimodel ensemble simulations of present-day and near-future tropospheric ozone, *J.Geophys.Res.*, *111*, D08301, doi:10.1029/2005JD006338, 2006

Thompson, A.M., Witte, J. C., McPeters, R. D., Oltmans, S. J., Schmidlin, F. J., Logan, J. A., Fujiwara, M., Kirchhoff, V. W. J. H., Posny, F., Coetzee, G. J. R., Hoegger, B., Kawakami, S., Ogawa, T., Johnson, B. J., Vömel, H. and Labow, G., Southern Hemisphere Additional Ozonesondes (SHADOZ) 1998-2000 tropical ozone climatology 1. Comparison with Total Ozone Mapping Spectrometer (TOMS) and ground-based measurements, J. Geophys. Res., Vol. 108 No. D2, 8238, doi: 10.1029/2001JD000967, 2003.

Van Aardenne, J. A., Dentener, F. J., Olivier, J. G. J., Klein-Goldewijk, C. G. M., and Lelieveld, J., A 1x1 degree resolution data set of historical anthropogenic trace gas emissions for the period 1890-1990, *Global. Biogeochem. Cycl.*, 15(4), 909-928, 2001.

Von Kulhmann, R., and Lawrence, M. G., The impact of ice uptake of nitric acid on atmospheric chemistry, *Atms. Chem. Phys., 6,* 225-235, 2006.

Walcek, C.J., Yuan, H-H, and Stockwell, W.R., The influence of aqueous-phase chemical reactions on ozone formation in polluted and non-polluted clouds, *Atms. Environ., 31(8),* 1221-1237, 1997.

Warneck, P., Chemistry of the Natural Atmosphere, International Geophysics Series, 71, Second Edition, Academic Press, San Diego, 927pp, ISBN 0-12-735632-0, 2000.

Williams, J. E., Dentener, F.J., and vanden Berg, A. R., The influence of cloud chemistry on HOx and NOx in the moderately polluted Marine Boundary Layer: a 1-D modeling study, *Atms. Chem. Phys., 2,* 39-54, 2002.

Williams, J. E., and van Noije, T. P. C., On the upgrading of the modified Carbon Bond Mechanism IV for use in global Chemistry transport Models, KNMI Scientific report WR 2008-02, pp 64, 2008.

Williams, J.E., Scheele, M. P., van Velthoven, P. F. J., Cammas, J-P., Thouret, V., Galy-Lacaux, C., and Volz-Thomas, A., *Atmos. Phys. Chem.,* 9, 5729-5749, 2009.

Van der Werf, G. R., Randerson, J. T., Giglio, L., Collatz, G. J., Kasibhatla, P. S., and Arellano Jnr, A. F., Interannual variability in global biomass burning emissions from 1997 to 2004, *Atms. Chem. Phys.,* 6, 3423-3441, 2006.

Van Zadelhoff, G-J., van Meijgaard, E., Donovan, D. P., Knap, W. H., and Boers, R., Sensitivity of the shortwave radiation budget to the parameterization of ice crystal radius, *J.Geophys.Res.*, 112, D08213, doi:10.1029/2006JD007791, 2007a.

Van Zadelhoff, G-J., Heymsfield, A. J., Donovan, D. P., and McGill, M. J., Evaluating lidar-radar microphysics retrieval using in-situ measurements, *J.Geophys.Res.*, 112, D09213, doi:10.1029/2006JD007202, 2007b.

All titles of KNMI-publications (and a full text PDF for the most recent ones) can be found on

# http://www.knmi.nl/bibliotheek/knmipub.html

*If you have any questions, please contact us: bibliotheek@knmi.nl*